BUBBLE DYNAMICS IN VIBRATED LIQUIDS UNDER NORMAL AND SIMULATED LOW GRAVITY ENVIRONMENTS

by

Daniel D. Kana

Wen-Hwa Chu

GPO PRICE $

CFSTI PRICE(S) $

Hard copy (HC) $3.00

Microfiche (MF) .65

ff 653 July 65

Technical Report No. 8
Contract No. NAS8-11045
Control No. TP 3-85175 & S-1 (1F)
SwRI Project No. 02-1391

Prepared for

National Aeronautics and Space Administration
George C. Marshall Space Flight Center
Huntsville, Alabama 35812

N67-30501
(ACCESSION NUMBER)

62
(PAGES)

CR-85575
(NASA CR OR TMX OR AD NUMBER)

(THRU)

1
(CODE)

12
(CATEGORY)

FACILITY FORM 602

15 February 1967

SOUTHWEST RESEARCH INSTITUTE
SAN ANTONIO HOUSTON

ABSTRACT

Bubble dynamics in vibrated liquids is studied both analytically and experimentally for normal and simulated low gravity conditions. Attention is focused on migration of bubbles to various locations within the tank when axisymmetric dynamic pressure conditions exist. A theory is developed to predict finite size bubble behavior, including natural frequencies of coupled axisymmetric modes of the system as well as average induced buoyancy force imparted to the bubble through the vibration. Calculated results are compared with experimental observations for a captive bubble in a vertically oriented tank and with results of a previous theory in which only small bubbles are allowed. It is found that small bubble theory is no longer valid for bubble-to-tank radius ratios greater than 0.05.

Additional experimental observations are performed in a horizontally oriented tank in which a captive bubble experiences zero gravity force in the horizontal direction. Longitudinal excitation of the system in this condition readily causes bubble migration to various points in the tank, even for very low acceleration inputs. Similar bubble behavior is displayed under random input conditions. It is concluded that low noise level accelerations can cause bubble migration under orbital conditions.

TABLE OF CONTENTS

LIST OF SYMBOLS

a	Inner radius of tank wall
a_s	Middle-surface radius of cylindrical tank wall
$A(x)$	Cross-sectional area of liquid at a given elevation in the tank (excludes area of bubble)
b	Unperturbed equilibrium radius of bubble
C_e	Effective sonic velocity through section of system that does not include the bubble
C_o	Sonic velocity in liquid alone
C_{eB}	Effective sonic velocity through section of system that includes the bubble
d_B	Bubble depth from liquid surface
E	Elastic modulus of tank
F	Induced buoyancy force on bubble under sinusoidal excitation
F_{avg}	Average induced buoyancy force on bubble under random excitation
g	Steady longitudinal acceleration
g_o	Standard acceleration of gravity
h	Wall thickness of tank
H	Liquid depth
p	Pressure at a given cross section in the cylindrical tank (assuming a plane-wave distribution)
p_o	Static ullage pressure in tank
p_l	Mean static pressure inside bubble
q	Longitudinal volumetric flow of liquid through a cross section A

r_B	Radial location of bubble
t	Time
u	Longitudinal velocity component of liquid
v_o	Unperturbed equilibrium volume of bubble
w	Radial displacement of tank wall
x	Axial coordinate relative to tank bottom
x_o	Excitational displacement amplitude
$( )^*$	Denotes a nondimensional variable
$(\hat{\ })$	Denotes the amplitude of an oscillatory variable
γ	Ratio of specific heats for bubble gas
Δ_B	Pulsating displacement of spherical bubble (Fig. 1b)
λ_i	Eigenvalue giving i-th natural frequency of combined liquid-bubble-elastic tank system
ξ	Axial coordinate relative to bubble center for unperturbed bubble (Fig. 1b)
ξ_1	Axial coordinate relative to bubble center for perturbed bubble (Fig. 1b)
ρ_L	Mass density of liquid
χ	Azimuth angle in bubble (Fig. 1b)
ω	Excitational frequency
ω_m	Central excitation frequency for 20-cps random bandwidth
ω_{oi}	Natural frequency for i-th axisymmetric mode of combined system
Ω_B	Natural frequency of bubble

LIST OF ILLUSTRATIONS

LIST OF ILLUSTRATIONS (Cont'd)

I. INTRODUCTION

The presence of bubbles in liquid propellants of space vehicles is well recognized to be a potential hazard to high-speed turbomachinery and a possible cause of excessive thrust fluctuations. Thus, it is essential that pure, bubble-free propellant be supplied to rocket engines at all times, including restarts from orbit as well as during launches from rest positions.

Because of the physical nature of cryogenic liquids and the space environment, the formation of bubbles within the body of liquid propellants occurs readily through several mechanisms. Normal boiling, liquid surface agitation, and nucleation caused by reduction of ullage pressure during venting operations are some of these mechanisms. The dynamic behavior of bubbles subsequent to their formation is then what determines whether they will vent into the ullage or will be caught into the outlet flow stream of the propellant during the boost phase, or whether they will vent or collect at undesirable locations within the tank while in the low gravity environment of the orbital phase.

Neglecting temperature gradient effects, it appears that there are three significant forces that influence the dynamic behavior of moving bubbles--the steady acceleration buoyancy, the drag force resulting from liquid viscosity, and an average induced buoyancy force which results from pressure oscillations within the liquid. Of these three, perhaps the vibrationally induced buoyancy force is currently the least understood.

Although the dynamic behavior of bubbles has long been the subject of numerous studies, it has only been within the last several years that bubble dynamics in space vehicle applications has been considered. One of the earlier reviews from this point of view was given by Dodge [1]†, who discussed all three forces affecting bubble motions. A much more recent discussion of bubble behavior under steady gravity and drag forces only has been given by Fritz [2], while Kana [3] has recently discussed how bubbles can influence the overall longitudinal vibration of a liquid-elastic tank system through their effect on the internal pressure distribution. These three papers have extensive reference lists on the subject. The relationship of bubble dynamics to overall liquid propellant problems has been discussed by Dachs [4]. He refers to the bubble coalescence phenomenon as CILIVIC (coalescence in liquids in a vibrating column).

† Numbers in brackets refer to the references cited at the end of the report.

Several investigations have been conducted to determine the effects of steady gravity and vibrational forces only. Although a number of investigators had observed peculiar behavior of bubbles and bubble clusters in vibrated tanks, Bleich [5, 6] was one of the first to correlate experimental observations with a theory developed for bubbles that are small relative to the tank dimensions. The results of this early investigation still appear to be one of the most useful methods of estimating bubble behavior, as will be shown later in the present report.

Kana and Dodge [7] found good correlation between the results of experimental observations and the predictions of Bleich's theory for small bubbles in elastic cylinders. It was found that the vibrational amplitude required to move small bubbles against a 1-g steady buoyancy was in general relatively large, but could be quite small in the vicinity of the natural axisymmetric modes of oscillation in the liquid-tank system. It was also shown experimentally that the bubbles tended to behave isothermally, rather than adiabatically. This result coincided with an earlier theoretical investigation of Plesset and Hsieh [8]. Subsequent to the work of Kana and Dodge [7], similar investigations were conducted by Fritz, et al. [9], and Schoenhals and Overcamp [10].

Although all of the previous work on bubble dynamics in vibrated liquids has been concentrated on the case of bubbles that are small relative to the tank dimensions, it has amply been shown that the oscillatory pressure distribution within the liquid is an inherent part of the problem. That is, bubble motion is influenced by both the amplitude and gradient of the pressure field at the bubble location. Thus, a variety of bubble behavior is possible, depending on the type and frequency of excitation that the system experiences. This situation is further complicated by the fact that the compliance of the bubble itself can influence this pressure distribution if its size becomes significant relative to the tank dimensions.

Kana [3] has pointed out that an elastic cylinder containing liquid can respond in several forms when excited by longitudinal vibration. However, only two forms of the response, one linear and one nonlinear, appear especially significant to bubble dynamics in that they can cause large axisymmetric pressure responses for relatively small longitudinal inputs. For the present, we shall consider only linear pressure fields. Several investigators recently have studied these linear axisymmetric modes of a longitudinally excited cylinder containing bubble-free liquid. An extensive reference list of this work appears in Reference [3]. A good knowledge of these modes of oscillation in the liquid-tank system is essential in that they form the exciting mechanism for the limiting case of small bubbles in a given system.

In all of the above work on bubble dynamics, little recognition has been given to the possible problems of bubble behavior in a low gravity environment or the effects of finite bubble size relative to the tank dimensions. The purpose of the present work is to delve further into these two aspects of the bubble dynamics problem. Possible bubble problems in a low gravity environment will be emphasized by showing that very small vibrational forces, such as can be induced by on-board support equipment in orbit, can move bubbles about, perhaps causing them to collect in undesirable locations, when only a weak steady buoyancy force is present. Thus, the average vibrational force will be specifically investigated by considering it to be completely independent of drag forces and only weakly dependent on gravity forces. Low gravity effects will be simulated by using counterbalanced captive bubbles, and it will be shown that random excitation, as well as sinusoidal excitation, has a strong influence on the bubble behavior. Only linear pressure responses under longitudinal excitation will be considered. A theory is developed for finite size bubbles, but it is shown by comparison that the much simpler theory of Bleich [5, 6] can be used for reasonable approximations of bubble behavior for smaller bubble sizes. Although in the present work the emphasis is on bubble behavior in low gravity environments, it is recognized that the results are also applicable to normal gravity conditions.

II. ANALYTICAL CONSIDERATIONS

Although this section includes an analytical development leading to the prediction of vibrational forces induced on finite size bubbles, the entire work is basically experimental, so that it emphasizes the techniques developed to simulate bubbles in a low gravity environment. The vibrational force induced on bubbles will be studied for longitudinal excitation both in a vertically oriented tank having a free surface and in a horizontally oriented tank without a free surface. However, the theory will be applied only to the vertically oriented tank. Therefore, this section begins with a discussion of pertinent variables involved in the physical system of the vertically oriented tank and the equations resulting from a dimensional analysis of them. Subsequently, the theoretical analysis of these variables then follows.

Dimensional Analysis

In the study of the behavior of bubbles under the influence of both steady buoyancy and vibrational forces in a vertically oriented and vibrated tank, ultimately the experiments can conveniently be separated into the determination of two independent variables. First, for a given bubble located at some point in the liquid in a specified elastic tank, one must determine the natural frequencies of the axisymmetric modes of oscillation of the combined system. The relationship of the exciting frequency to these natural modes then has a profound influence on the induced vibrational force experienced by the bubble in the forced system.

Thus, a coupled natural frequency parameter can be expressed as

$$\frac{\omega_{oi}a}{C_o} = \mathcal{J}_1\left[\frac{d_B}{H}, \frac{r_B}{a}, \frac{H}{a}, \frac{b}{a}, \frac{p_o}{\rho_L g_o a}, \gamma, \frac{C_o^2}{g_o a}, \frac{C_e}{C_o}, \frac{g}{g_o}\right] \qquad (1)$$

where the use of the equivalent sonic velocity C_e implies the existence of a plane wave pressure distribution in the liquid-elastic tank column when a bubble is not present. This approximation has been shown to be valid [11] for liquid depths only in the range $H/a > 2$ along with the range of other variables which we will be considering. Upon determining the natural frequency ω_{oi} of the system, then, for the forced vibration problem, the average induced vibrational force can be expressed as:

$$\frac{F}{\rho_L g_o v_o} = \mathcal{J}_2\left[\frac{d_B}{H}, \frac{r_B}{a}, \frac{H}{a}, \frac{b}{a}, \frac{p_o}{\rho_L g_o a}, \gamma, \frac{\omega_{oi} a}{C_o}, \frac{\omega}{\omega_{oi}}, \frac{x_o \omega^2}{g_o}, \frac{g}{g_o}, \frac{C_e}{C_o}, \frac{C_o^2}{g_o a}\right] \quad (2)$$

Equations (1) and (2) show all the variables considered pertinent in the present study. It is ovbious that viscous and surface tension effects are not included, and the force exerted on the bubble in a static position will be studied. The force parameter given in Equation (2) is the ratio of the induced vibrational force to the static buoyancy force resulting from a 1-g_o axial acceleration.

Finite Size Bubble Theory

Natural Frequencies of the System. If the circular cylindrical elastic shell is considered to be a membrane [12], its governing equation can be written as

$$\ddot{w} + \frac{E}{\rho_s a_s^2} w = \frac{p}{\rho_s h} \quad (3)$$

while the bubble equation [5] can be written as

$$\ddot{\Delta}_B + \Omega_B^2 \Delta_B = \frac{-p}{\rho_L b} \quad (4)$$

where the bubble natural frequency is given as†

$$\Omega_B^2 = \frac{3\gamma p_1}{\rho_L b^2} \quad \text{and} \quad p_1 = p_o + \rho_L g d_B \quad (5)$$

Equations (3) and (4) are the governing equations for the shell and bubble, respectively. It is further necessary to have such an equation governing the liquid. For this analysis, we shall apply quasi-one-dimensional equations to the liquid region between the bubble and the shell (this assumption has already been made for those regions where no bubble exists, as was indicated above in the use of the equivalent sonic velocity C_e). The tank coordinate system is shown in Figure 1a, while the bubble coordinate system is shown in

†It should be noted that surface tension effects are not included in this expression.

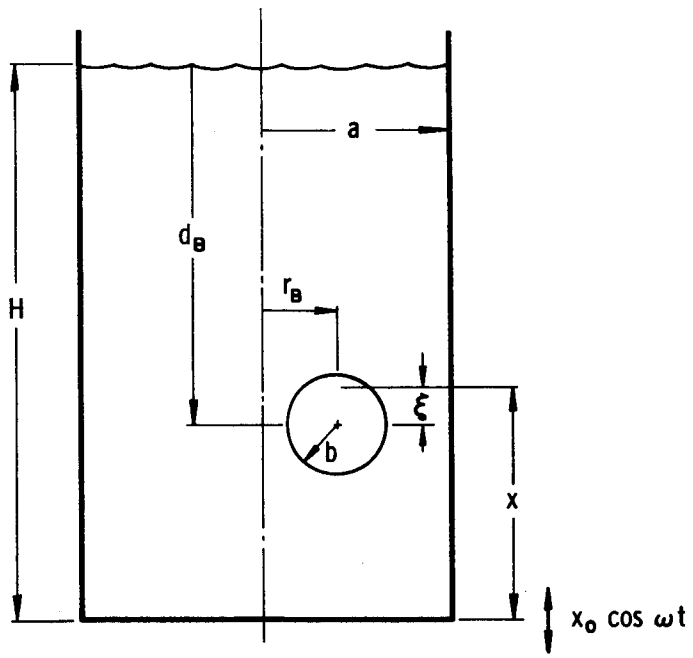

Figure 1a. Tank coordinate system

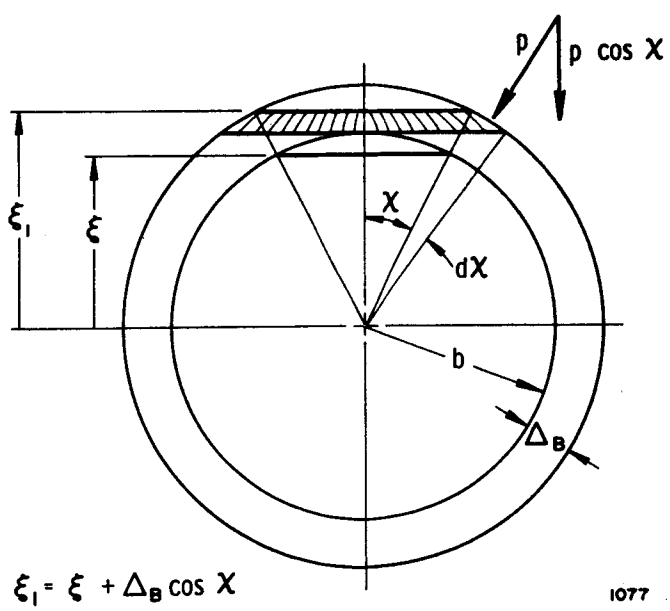

Figure 1b. Bubble coordinate system

Figure 1b. Analogous to Tarantine [13], the average of the linearized continuity equation yields

$$\frac{\partial \rho}{\partial t} + \frac{\rho_L}{A}\frac{\partial q}{\partial x} + \frac{2\pi\rho_L}{A}\left(a\frac{\partial w}{\partial t} - b\sin^2\chi\frac{\partial \Delta_B}{\partial t}\right) = 0 \tag{6}$$

where q is the volumetric flow $\int udA$, and A is the cross-sectional area. For theoretical purposes, we will consider only the case of $r_B = 0$, where the bubble is located on the centerline of the tank. The development of Equation (6) appears in the Appendix. Similarly, the linearized momentum equation is

$$\frac{\partial p}{\partial x} \cong -\frac{\rho_L}{A(x)}\frac{\partial q}{\partial t} \tag{7}$$

Now, assuming the existence of periodic motion and using Equations (3) and (4) to eliminate w and Δ_B from Equation (6), we have

$$\frac{1}{C_{eB}^2}\frac{\partial p}{\partial t} = -\frac{\rho_L}{A}\frac{\partial q}{\partial x} \tag{8}$$

where

$$C_{eB}^2 = \frac{C_o^2}{\left[1 + \rho_L\frac{C_o^2 2a_s}{A^* hE} + \frac{2C_o^2\sin^2\chi}{a^2A^*(\Omega_B^2 - \omega^2)}\right]} \tag{9a}$$

$$\sin^2\chi = 1 - \frac{\xi^{*2}}{\left(\frac{b}{a}\right)^2} \tag{9b}$$

$$A^* = \left[1 - \frac{b^2}{a^2} + \xi^{*2}\right] \tag{9c}$$

These equations are valid in the range

$$-\frac{b}{a} < \xi^* < \frac{b}{a}$$

It may be noted that C_{eB} can be considered an effective sonic velocity in the above range of ξ^* (i.e., in a cross section that cuts through the bubble), and that outside this range it becomes

$$C_{eB}^2 \equiv C_e^2 = \frac{C_o^2}{\left[1 + \rho_L C_o^2 \frac{2a_s}{hE}\right]} \tag{10}$$

the effective sonic velocity in an elastic tank in which no bubble is present. If $\Omega_B^2 < \omega^2$ and $\Omega_B^2 - \omega^2$ is small, then C_{eB} becomes imaginary, and it can no longer be interpreted as an effective sonic velocity.

Equations (7) and (8) can be combined to give the nondimensional equation

$$\frac{\partial^2 p^*}{\partial x^{*2}} + \frac{1}{A^*}\frac{\partial A^*}{\partial x^*}\frac{\partial p^*}{\partial x^*} + \frac{1}{C_{eB}^{*2}}\left(\frac{\omega^2 a^2}{C_o^2}\right) p^* = 0 \tag{11a}$$

where

$$C_{eB}^* = \frac{C_{eB}}{C_o} \tag{11b}$$

$$p^* = \frac{p}{\rho_L g_o a} \tag{11c}$$

$$x^* = x/a \tag{11d}$$

The boundary conditions are

$$p^* = 0 \text{ at } x^* = H/a$$

and

$$\frac{\partial p^*}{\partial x^*} = -\frac{x_o \omega^2}{g_o} \cos \omega t \text{ at } x^* = 0$$

In order to solve Equations (11) for the pressure p^*, it is necessary to use a numerical solution. Details of such a numerical solution are given in the Appendix. In essence, Equations (11) reduce to a matrix equation

$$\left\{[A] - \lambda^2[B]\right\}[P] = [C] \tag{12a}\dagger$$

†[A], [B], [C] are matrices, the elements of which are given in the Appendix.

where

$$\lambda^2 = \frac{\omega^2 a^2}{C_o^2}$$

The natural frequencies of the combined system are then obtained from the determinant

$$\left|[A] - \lambda_1^2[B]\right| = 0 \tag{12b}$$

The lowest eigenvalue is determined by repeated linear interpolation of the determinantal equation. Standard eigenvalue subroutines are not applicable since [B] depends on the frequency ω, thus on λ.

Average Force on Bubble. In view of the variables shown in Figure 1b, the time average of the vertical component of force that results from the integration of pressure over the bubble surface can be expressed as

$$F = -2\pi \int_0^{\pi} \overline{p(\xi_1)(b + \Delta_B)^2 \sin\chi \cos\chi \, d\chi}$$

The evaluation of this integral is given in the Appendix. The final nondimensional result for the induced buoyancy force is

$$\frac{F}{\rho L g_o v_o} = -\frac{3}{4}\frac{a^2}{b^2}\left[(\hat{p}^*)_{\xi^* = b/a} - (\hat{p}^*)_{\xi^* = -b/a}\right]\hat{\Delta}_B^* \tag{13a}$$

where

$$\hat{\Delta}_B^* = \frac{\hat{\Delta}_B}{a} = \frac{a}{b}\,\frac{P_1^*}{\left(1 - \frac{\Omega_B^2}{\omega^2}\right)} \tag{13b}$$

and

$$P_1^* = \frac{1}{2}\int_0^{\pi} \hat{p}^* \sin\chi \, d\chi \tag{13c}$$

Here, v_o is the equilibrium volume of the bubble, and it is understood that $(\hat{})$ represents the amplitude of an oscillatory variable. The evaluation of Equations (13) must be carried out using a numerical process. The formulation of this process is given in the Appendix.

Small Bubble Theory

For the case of bubbles that are small relative to the tank dimensions, the above theory must necessarily reduce to that of Bleich [5] as applied to a quasi-one-dimensional (plane wave) approximation [7]. Thus, Equation (11a) reduces to the nondimensional wave equation, and, as given in Reference [7], natural frequencies of the closed-open elastic tank containing liquid can be approximated by

$$\frac{\omega_{oi} H}{C_e} = (2i - 1)\ \frac{\pi}{2} \tag{14}$$

Then, in order to determine the induced vibrational force on the small bubbles, from Equations (13), we have

$$(\hat{p}^*)_{\xi^* = b/a} - (\hat{p}^*)_{\xi^* = -b/a} \cong 2\ \frac{b}{a}\ \frac{\partial \hat{p}^*}{\partial \xi^*}$$

$$\hat{\Delta}^*_{BO} = \frac{a}{b}\ \frac{\hat{p}^*}{\left(1 - \dfrac{\Omega_B^2}{\omega^2}\right)}$$

and the average nondimensional induced buoyancy force is

$$\frac{F}{\rho_L g_o v_o} = -\frac{3}{2}\ \frac{a^2}{b^2}\ \frac{\hat{p}^*}{\left(1 - \dfrac{\Omega_B^2}{\omega^2}\right)}\ \frac{\partial \hat{p}^*}{\partial \xi^*} \tag{15}$$

which is the equation developed in Reference [7], providing that we introduce

$$\xi^* = \frac{\xi}{a} = \frac{1}{a}\,(d_B - z)$$

Upon using the one-dimensional wave equation to obtain the pressure and pressure gradient as was done in Reference [7], and using Equation (5), Equation (15) can be expressed in terms of the variables in Equation (2) as follows:

$$\frac{F}{\rho_L g_o V_o} = -3 \frac{\left(\frac{H}{a}\right)\left(\frac{x_o\omega^2}{g_o}\right)^2 \sin\left(\pi \frac{d_B}{H} \frac{\omega}{\omega_{o1}}\right)}{\left(\pi \frac{\omega}{\omega_{o1}}\right)\left[1+\cos\left(\pi \frac{\omega}{\omega_{o1}}\right)\right]\left[3\gamma\left(\frac{p_o}{\rho_L a g_o} + \frac{g}{g_o}\frac{d_B}{H}\frac{H}{a}\right) - \frac{b^2}{a^2}\frac{\omega_{o1}a^2}{C_o^2}\frac{C_o^2}{g_o a}\frac{\omega^2}{\omega_{o1}^2}\right]} \tag{16}$$

This expression gives a useful relationship for estimating the average induced buoyancy force for small bubbles in any gravity environment. It is desirable to determine the bubble parameters at which the results predicted by Equations (13) begin to deviate from those predicted by Equation (16).

In order to study the interaction of the induced average buoyancy force given by Equation (16) and a steady, but small gravity force, it is convenient to combine the two forces so that positions of bubble equilibrium (stable or unstable) are determined in a vertically vibrated tank. This has already been done for large steady gravity forces in Equation (19) of Reference [7]. By changing the variables in this equation to include all those given in Equation (2) of the present report, we have

$$\frac{x_o\omega^2}{g_o} = \left\{ \frac{2\gamma\left(\frac{g}{g_o}\right)\left(\frac{g}{g_o} + \frac{H}{d_B}\frac{p_o}{\rho_L a g_o}\frac{a}{H}\right)}{\frac{2\sin\left(\pi \frac{d_B}{H}\frac{\omega}{\omega_{o1}}\right)}{\pi \frac{d_B}{H}\frac{\omega}{\omega_{o1}}\left[1+\cos\left(\pi \frac{\omega}{\omega_{o1}}\right)\right]}} \right\}^{1/2} \tag{17}$$

But, for

$$\frac{g}{g_o} \ll \frac{H}{d_B}\frac{p_o}{\rho_L a g_o}\frac{a}{H}$$

this becomes

$$\frac{x_o\omega^2}{g_o} = \sqrt{\frac{g}{g_o}} \left\{ \frac{2\gamma \frac{H}{d_B}\frac{p_o}{\rho_L a g_o}\frac{a}{H}}{\frac{2\sin\left(\pi \frac{d_B}{H}\frac{\omega}{\omega_{o1}}\right)}{\pi \frac{d_B}{H}\frac{\omega}{\omega_{o1}}\left[1+\cos\left(\pi \frac{\omega}{\omega_{o1}}\right)\right]}} \right\}^{1/2} \tag{18}$$

Equation (18) gives the input acceleration required to cause a small bubble to be in equilibrium at a given depth d_B in a vertically oriented and vibrated elastic tank. It should also be noted that in this expression an assumption has been made that

$$\omega << \Omega_B$$

III. EXPERIMENTAL APPARATUS

The apparatus used for the experiments of the present study is shown in the photographs of Figures 2 through 4. Basically, the same apparatus was used for both the vertically and horizontally oriented tanks, except for the bulkheads on the tank and some parts of the instrumentation. Similar types of counterweighted captive bubbles were used in both cases, and water was used for the model liquid.

Vertical Orientation

Figure 2 shows the vertically oriented tank containing a captive bubble. The Lucite tank (E = 800,000 psi) had a mean diameter of 25.1 cm, was 50.3 cm long, and had a wall thickness of 3.18 mm. Thus, the inner radius was 12.4 cm. All vertical tests were run with a water depth of H/a = 3.69. The tank is shown with its lower flange mounted on a rigid flat bottom that is bolted directly to the shaker armature.

The captive bubble is made of a thin rubber balloon with an air valve at the bottom. Thus, the amount of air in the balloon could be adjusted. The balloon was counterweighted to be exactly neutrally buoyant in a 1-g_o field at the depth that force measurements were taken. This balloon-counterweight system was attached to a thin cantilever beam force transducer which was fixed to a rod that extended down into the tank. The force transducer had one semiconductor strain gage on top and one on the bottom of the beam near its root. High sensitivity of the semiconductor gages and associated instrumentation allowed force readings to within about 10 dyn. Pressure distributions in the liquid were measured by means of a miniature pressure transducer mounted in the 3.8-mm diameter rod that extends into the left side of the tank in Figure 2. Referring to Equations (1) and (2), the tests for the vertically oriented tank were conducted so that the following parameters were held constant unless otherwise noted on the results:

$$\frac{H}{a} = 3.69, \quad \frac{P_o}{\rho_L g_o a} = 85.8, \quad \frac{C_o^2}{g_o a} = 1.67 \times 10^6$$

$$\gamma = 1.0, \quad \frac{C_e}{C_o} = 0.184, \quad \frac{g}{g_o} = 1.0$$

Other independent parameters in Equations (1) and (2) were varied in order to determine their influence on the natural frequencies and average induced buoyancy force.

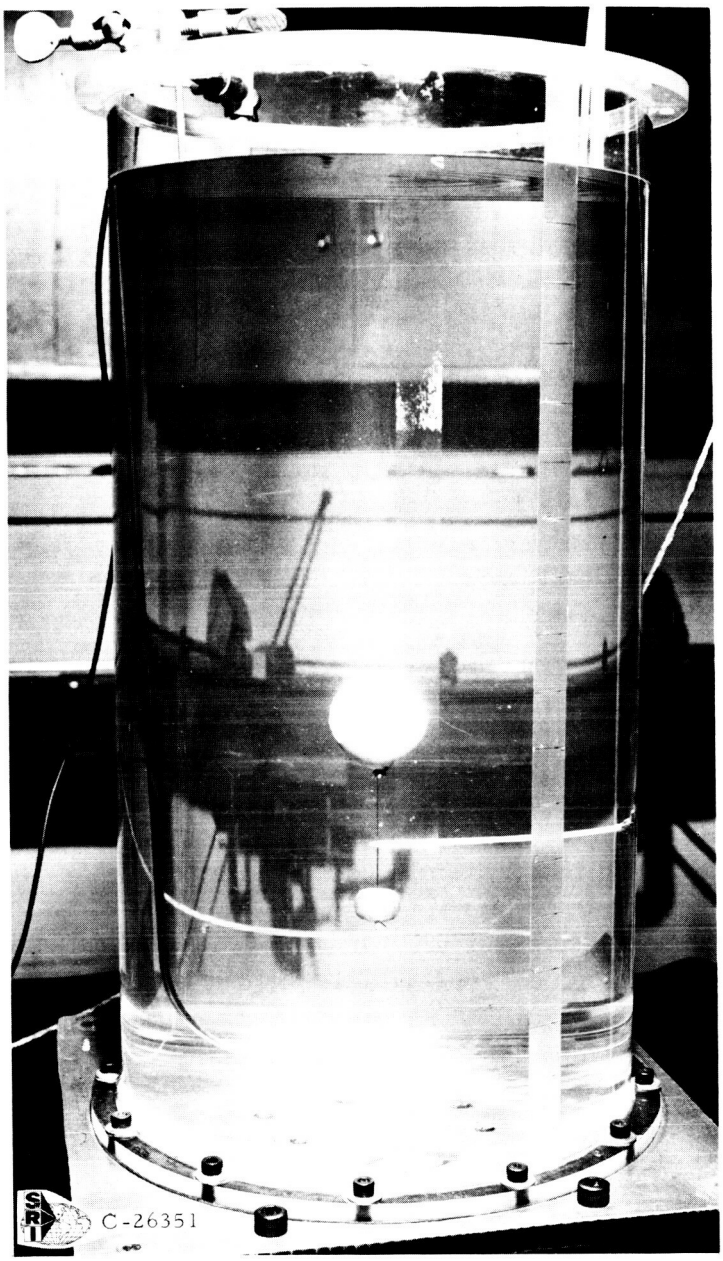

Figure 2. Captive bubble in vertical tank

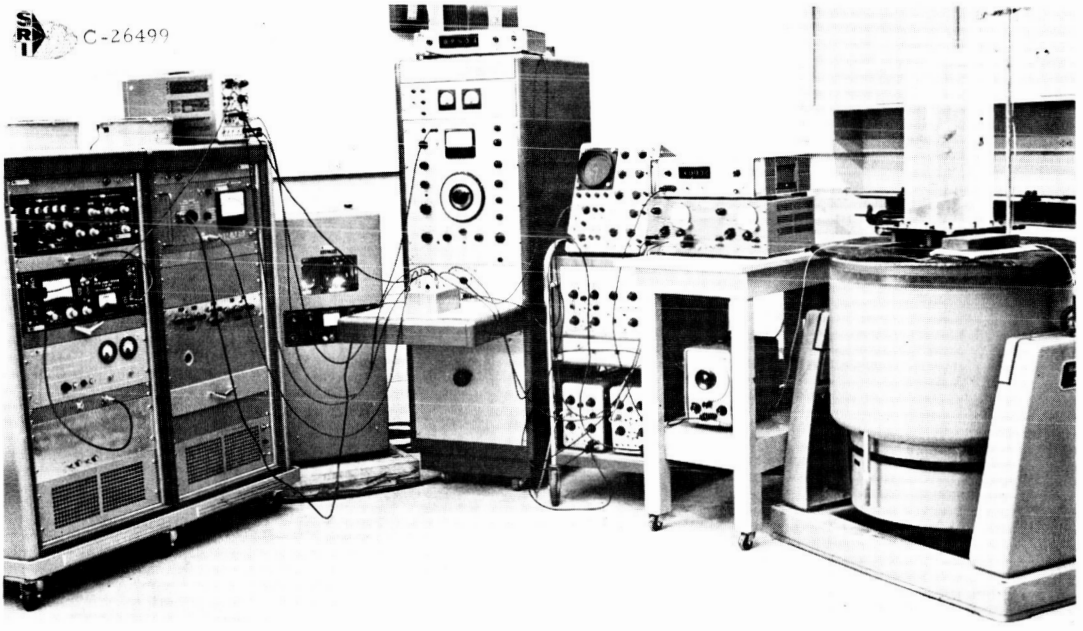

Figure 3. Overall experimental apparatus

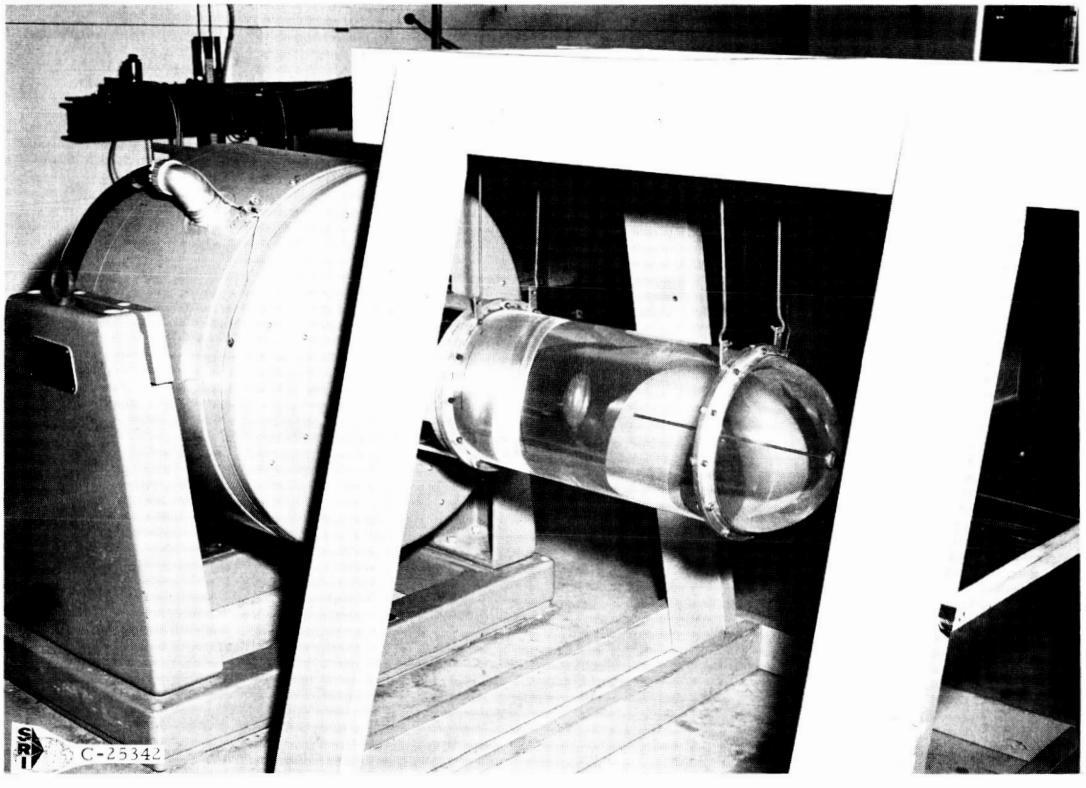

Figure 4. Captive bubble in horizontal tank

A photograph of the overall apparatus is shown in Figure 3, while simplified diagrams of the instrumentation are shown in Figures 5 and 6. It can be seen that the instrumentation for sinusoidal excitation is considerably simpler than that for random excitation. In both cases, the force signal is filtered to remove dynamic components so that only the desired average signal could be read on a DC digital voltmeter. The dynamic signal did not represent the true dynamic buoyancy force since some dynamic signal was generated by the liquid pressure acting on the beam alone; however, the average force was that from the bubble only.

It can be seen from Figure 6 that a somewhat restricted form of random excitation was used. That is, a relatively narrow band (3-db bandwidth of 20 cps) of random signal was used as the excitation for this case. This particular form of random signal was used since the average bubble force that it produced could more directly be compared with that obtained from the sinusoidal excitation when the center frequency of the bandwidth was set equal to the frequency at which sinusoidal data were obtained. Input acceleration was measured in rms-g's by using the instrumentation indicated. The excitation signal was applied for 25 sec and integrated to obtain the rms value. The force signal, which varied somewhat during this time, was averaged by sight reading of the digital voltmeter and oscilloscope. The 25-sec averaging period was determined to be adequate to produce a 95-percent confidence level in the measured values.

Horizontal Orientation

A photograph of the horizontally oriented tank has been shown in Figure 4. The cylinder which formed the center portion of this tank was the same as that previously described; however, here it was fitted with Lucite hemispherical bulkheads on both ends. These bulkheads were blown from heated 3.18-mm thick Lucite sheets, and varied in thickness to 1.59 mm at the center after formation. Horizontal longitudinal excitation was provided through a circular bracket attached to one flange of the tank. Four vertical supports were used to absorb the deadweight of the entire system.

For this orientation, the captive bubble was counterweighted to where it was just neutrally buoyant on the centerline of the tank. This reduced friction at the contact point between the weights and the tank wall. Thus, the bubble was free to move under any horizontally applied force. The weights were made of steel so that an external bar magnet could be used to move the bubble to different positions in the tank. Of course, all adjustments in bubble size and counterweights had to be made while one end of the tank was open and setting vertically.

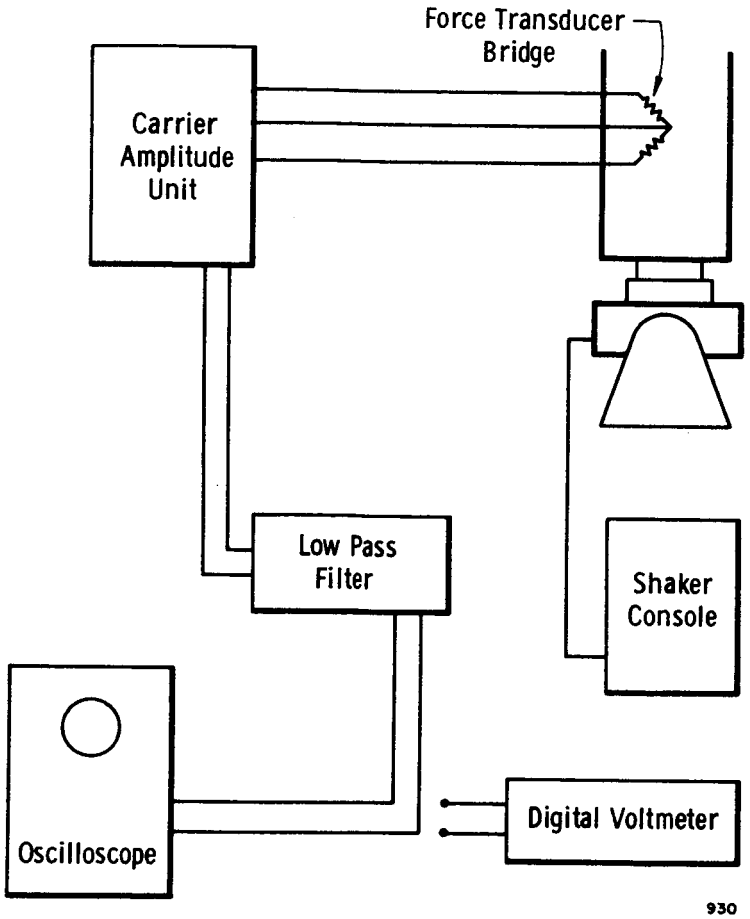

Figure 5. Sketch of instrumentation for sinusoidal excitation

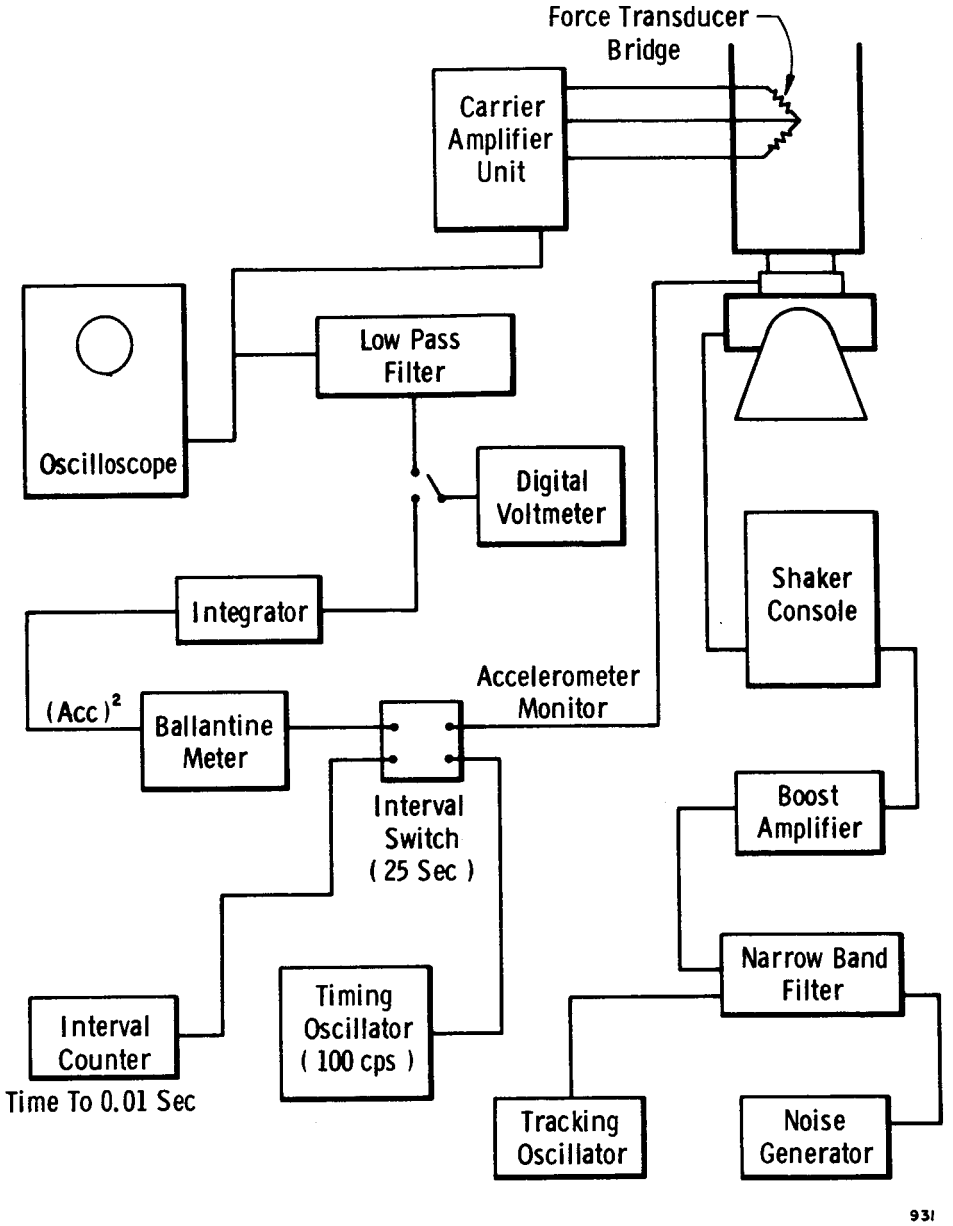

Figure 6. Sketch of instrumentation for random excitation

As can be seen from Figure 4, a pressure probe similar to that previously described was used for measuring pressure distributions. Here, the probe was straight and was inserted into the tank through a rubber plug at the center of the free-end bulkhead. Force measurements were not taken on the captive bubble since this would have required a considerably more elaborate force transducer design because of the inaccessible location of the bubble for this condition. However, a qualitative indication of the force could readily be obtained by visually observing how rapidly the bubble moved from a given initial position for given excitational conditions.

IV. THEORETICAL AND EXPERIMENTAL RESULTS

Vertical Orientation

Natural Frequencies of System. The importance of the axisymmetric modes of oscillation on bubble dynamics in a longitudinally excited tank has already been emphasized. Figure 7 shows the pressure distribution for the first two of these modes as they occur for bubble-free liquid in the present experimental system. It may be anticipated that the presence of a small bubble at various axial locations in the tank would cause only insignificant distortions in the shape of this pressure as well as insignificant changes in the natural frequency, whereas larger bubbles would cause marked changes in both. Evidence of the influence of both bubble size and axial position on the natural modes of the system containing a bubble is shown in Figures 8 and 9.

Figure 8 shows both theoretical and experimental values of natural frequency for the first mode only. The theoretical values obtained for the two larger bubbles were computed numerically from Equation (12) using twenty increments (N = 20) across the bubble, while the small bubble theory values were obtained from Equation (14). It may be recalled that small bubble theory assumes the existence of a plane water-hammer wave that is not influenced by the presence of a bubble. Thus, as would be expected, only the experimental values for the smallest bubble correlate well with these values. For the two larger bubbles, it can be seen that good correlation is obtained with the finite bubble theory, with the best correlation occurring for the largest bubble. For the smallest bubble, numerical results from the finite bubble theory involved an error of about 20 percent, and, in one case, it failed to converge within thirty iterations. In view of this trend, it is believed that the discrepancy results principally from the form [Eq. (5)] of the theoretical coupled bubble frequency (Ω_B) used in computing the theoretical frequency (ω_{oi}) of the combined system. More accurate results probably could be obtained by including surface tension terms (particularly for a captive bubble made from a rubber balloon). Use of a smaller mesh size in the numerical process probably would also improve the results.

A similar dependence of natural frequency on bubble size and axial position is shown in Figure 9 for the second mode. No theoretical results were computed for this mode. It is obvious from the results for both modes that the concentrated compliance of a bubble produces the most significant change in frequency when it is located near an antinode of the pressure distribution of a given mode. Although the shape of the pressure wave was not determined with a bubble present, it would be expected that the most distortion would occur with the bubble at these locations; with the bubble near a

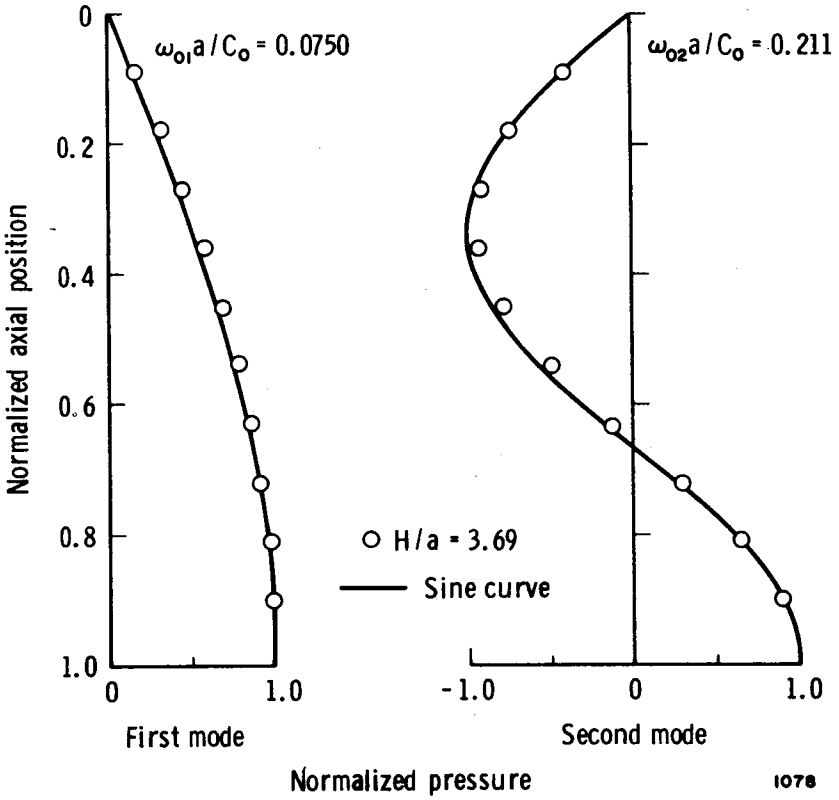

Figure 7. Pressure distribution for first two axisymmetric modes in vertical tank without bubble

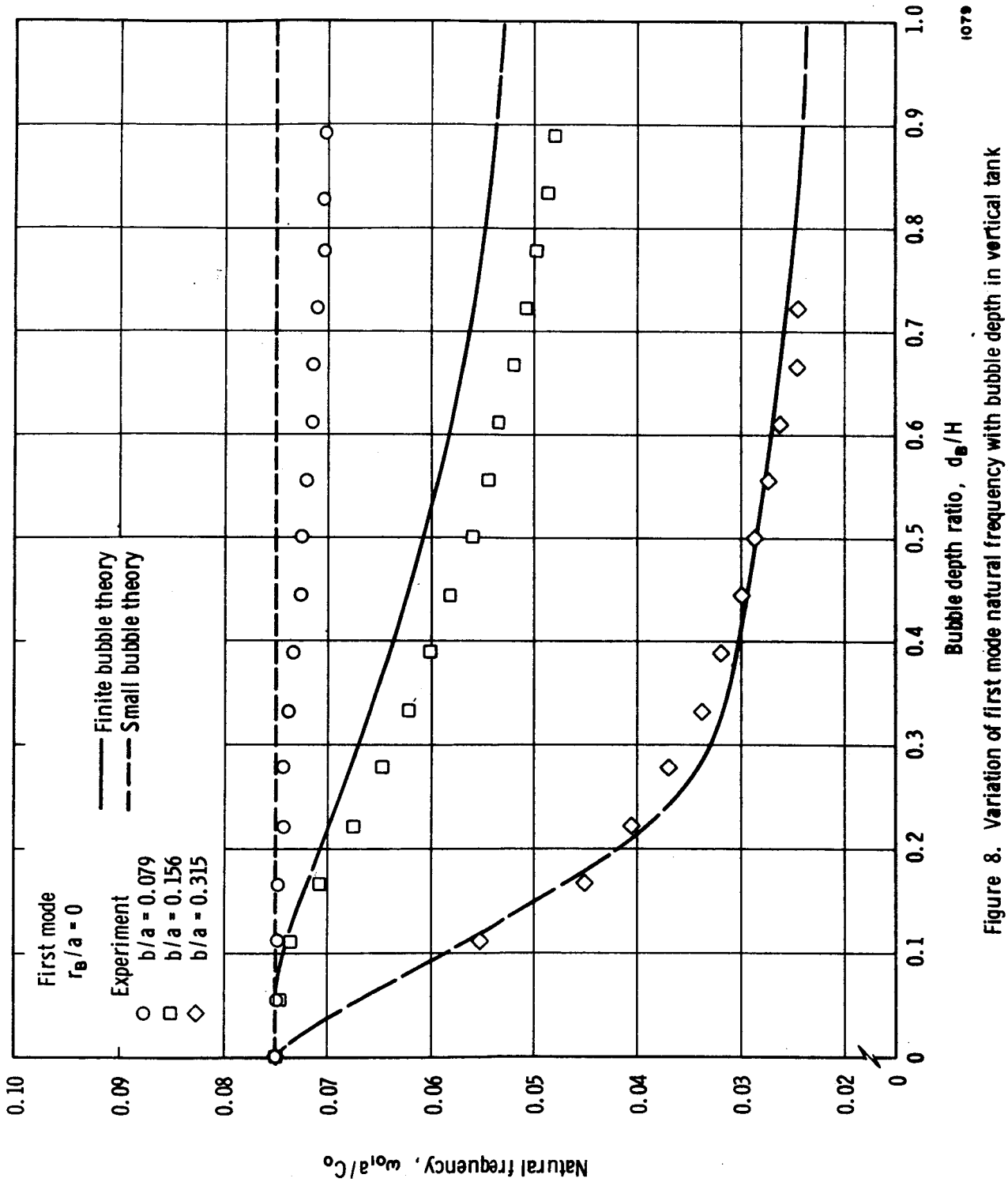

Figure 8. Variation of first mode natural frequency with bubble depth in vertical tank

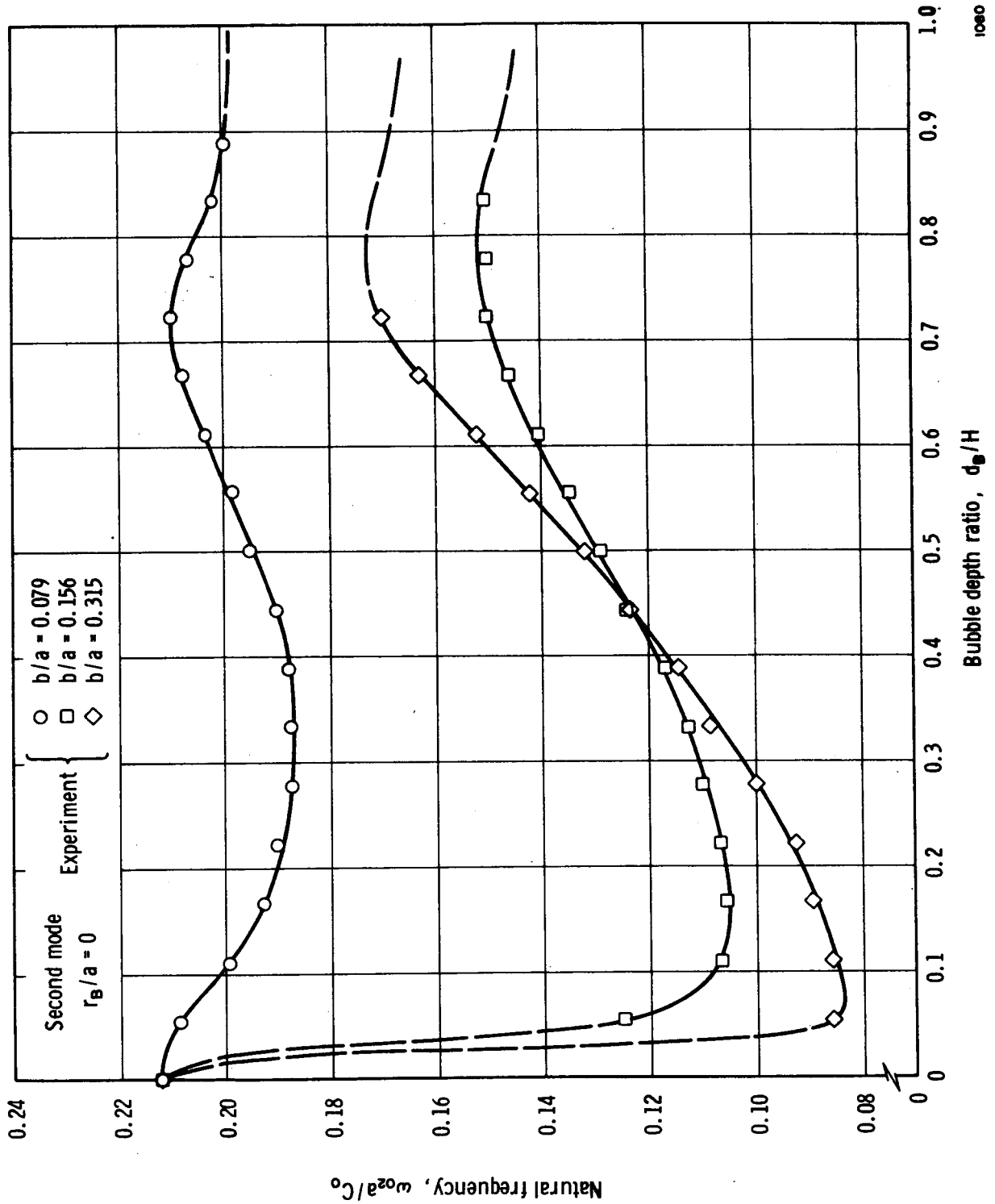

Figure 9. Variation of second mode natural frequency with bubble depth in vertical tank

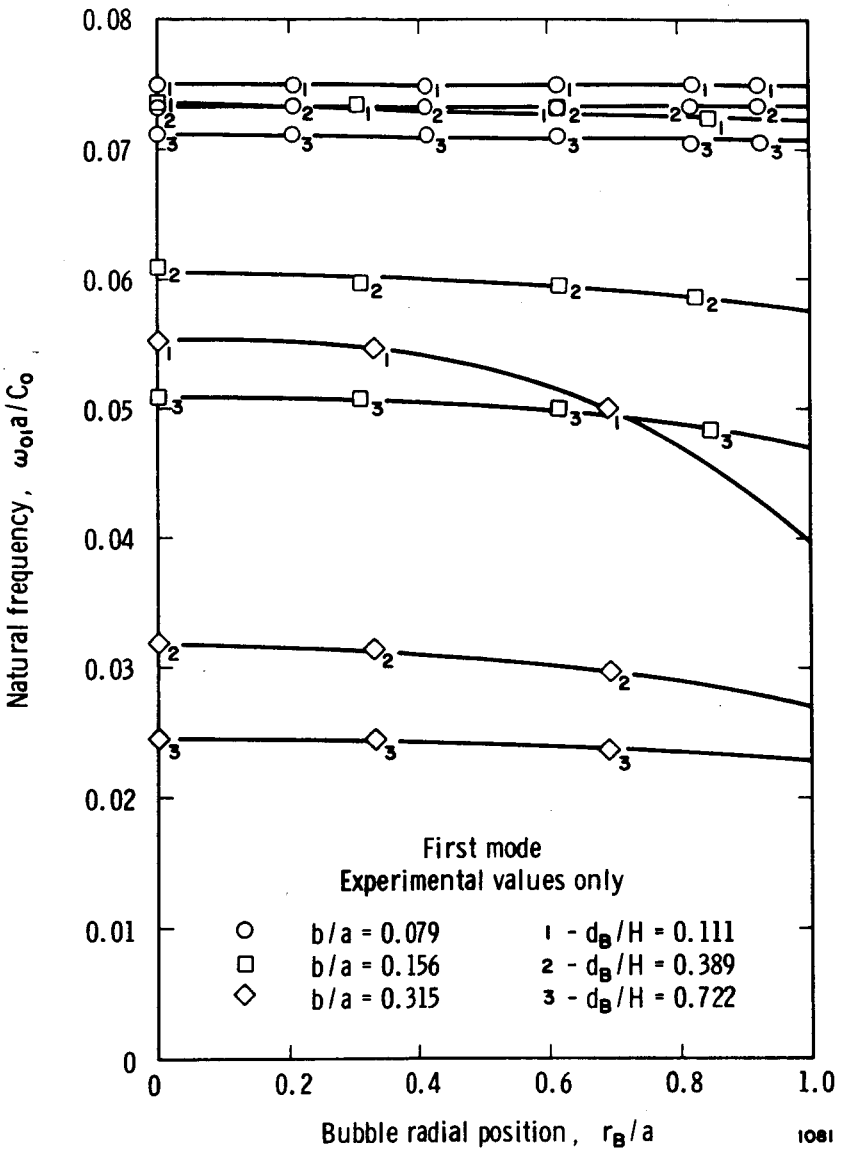

Figure 10. Variation of first mode natural frequency with radial position of bubble in vertical tank

node, the pressure wave for the first two modes would look essentially like those in Figure 7. These results show that a bubble size of about $b/a = 0.05$ is the limit above which the small bubble theory no longer gives a good approximation to the natural frequency of the system, while the finite bubble theory does not appear to give useful results below this limit.

The data in Figures 8 and 9 were all obtained for bubbles located along the central axis of the cylindrical tank. The effect of an eccentric bubble position on natural frequency is shown for the first mode only in Figure 10. Of course, the values at $r_B/a = 0$ correspond to values from Figure 8. Only the largest bubble appeared to cause significant change in natural frequency as the bubble radial position was varied. The experimental data were taken only for points where the bubble did not touch the wall of the tank.

Bubble Force for Sinusoidal Excitation. Theoretical and experimental correlation for the average induced buoyancy force on a medium sized bubble is shown in Figure 11 for several bubble depths. Input acceleration was held constant, while frequency was varied. The theoretical results are based on a numerical solution of Equations (13). It can be seen that good agreement is achieved, except at higher frequencies, for the smallest bubble depth. At this point, the theoretical coupled natural frequency [Ω_B given by Eq. (5)] of the bubble itself influences the results. Apparently, this natural frequency never occurred in the experimental system at the predicted value. It has been mentioned that including surface tension effects probably would improve the results. This may not be surprising since the theory assumes the presence of a pure gas bubble, and the captive bubble, having been made from a rubber balloon, could at best only approximate the assumed form and would include grossly exaggerated surface tension effects because of the elasticity of the balloon. The trend of the data, which shows greater discrepancies for converging bubble frequency and system frequency, is consistent with that shown in Figure 8.

The marked influence of the bubble mode on the induced buoyancy force as indicated by the theoretical curve in Figure 11 does not appear to occur experimentally. However, the effect of the coupled axisymmetric mode of the combined system is vividly displayed by the peak which occurs at the natural frequency for this mode. It should be emphasized that the force parameter is based on a $1\text{-}g_o$ steady acceleration, and, although the indicated values are small, they can be quite significant under certain conditions, as will be shown in the subsequent figures.

Additional experimental data for induced buoyancy force are shown in Figure 12 for the same bubble and depths indicated above. However, here

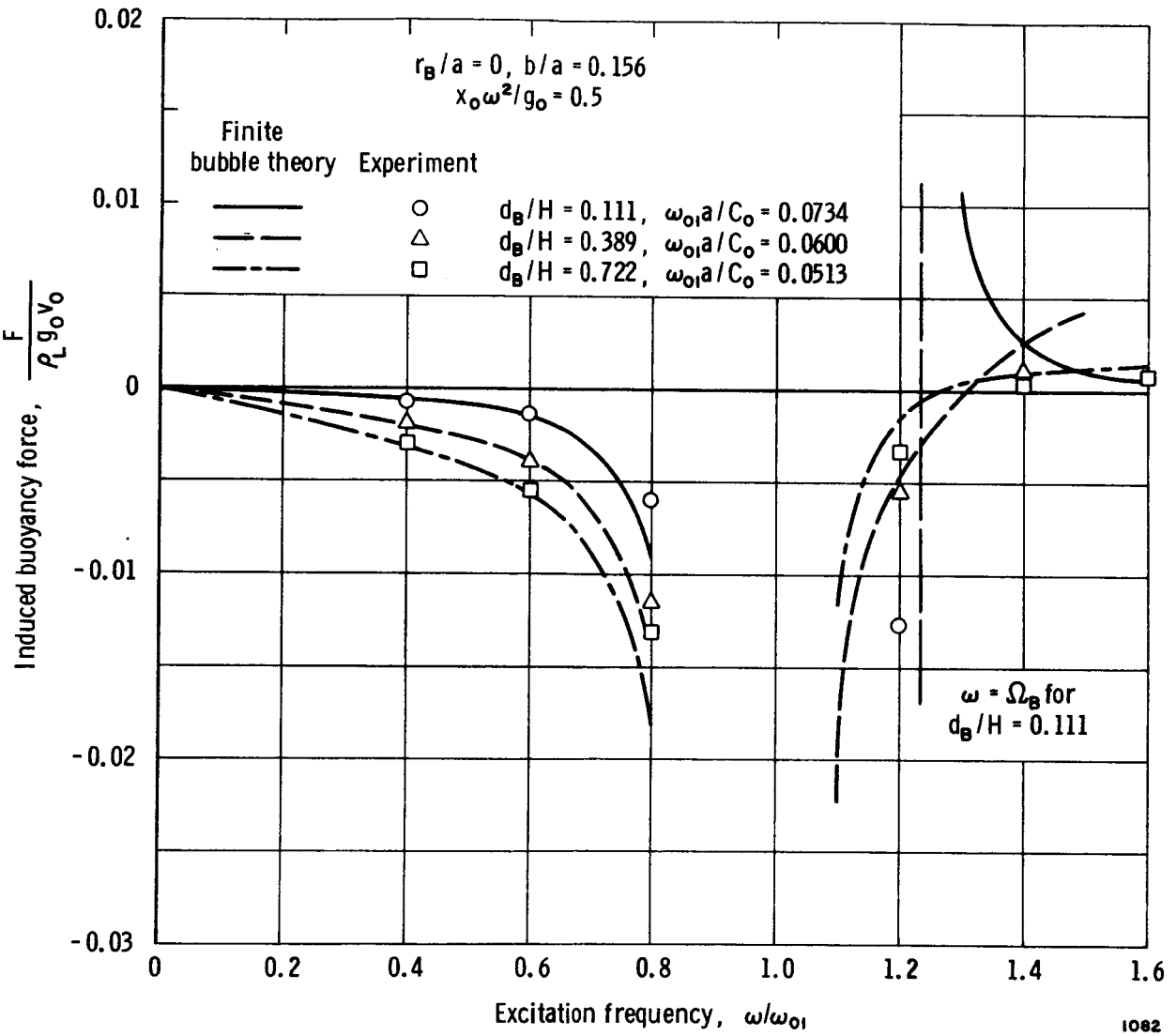

Figure 11. Influence of excitational frequency on induced buoyancy force on bubble in sinusoidally excited vertical tank

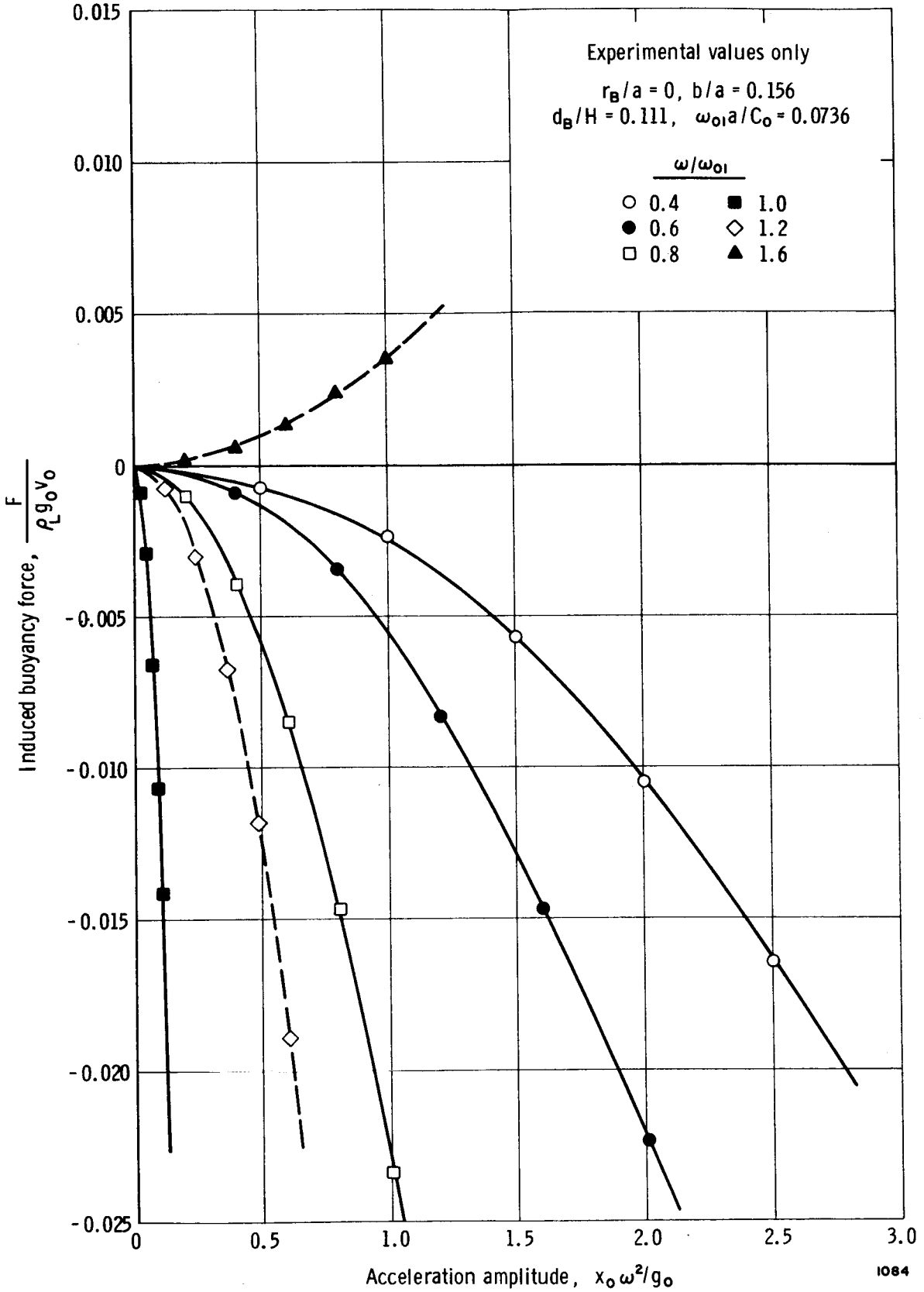

Figure 12a. Influence of excitational acceleration on induced buoyancy force on bubble in sinusoidally excited vertical tank
(Bubble near liquid surface)

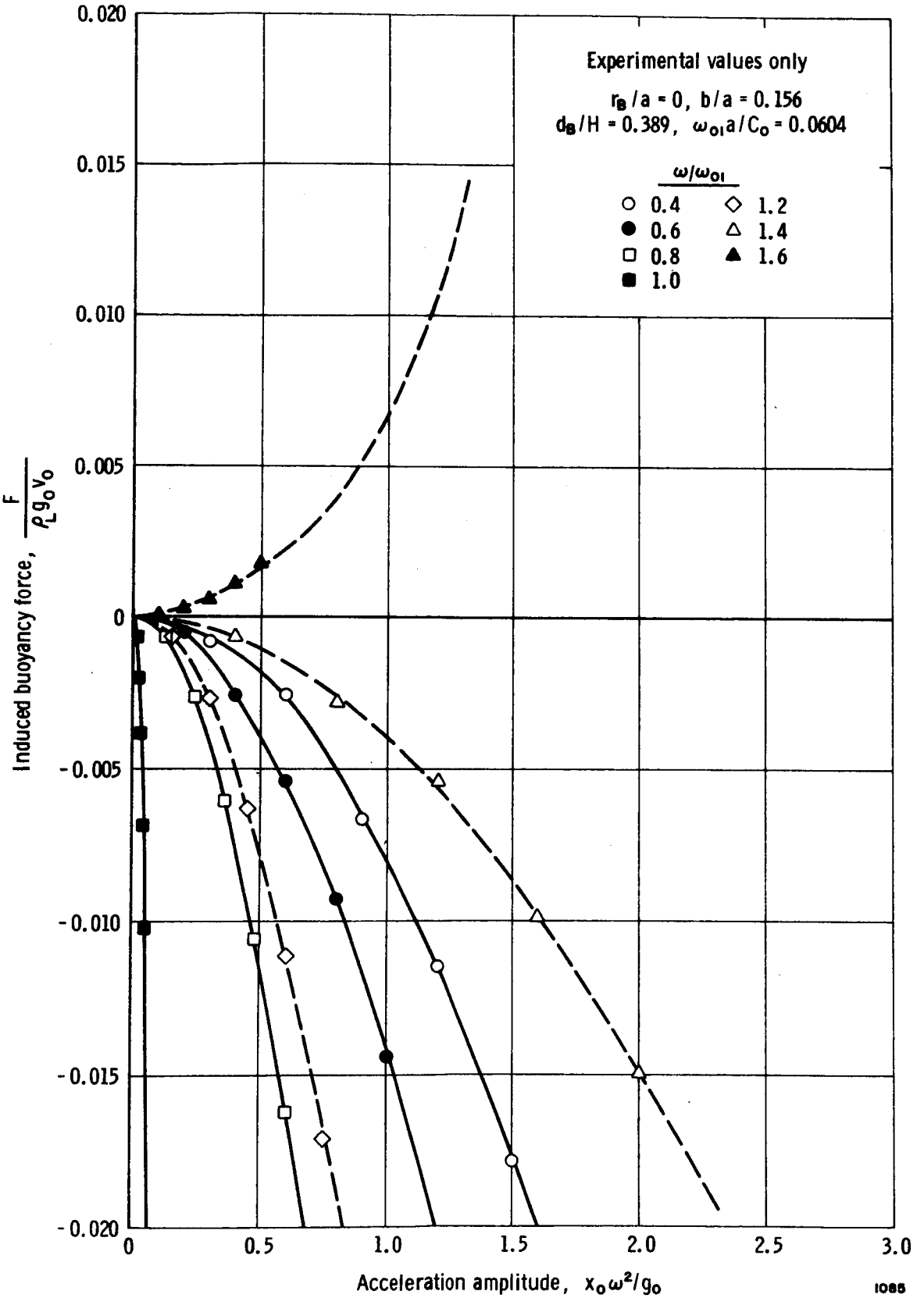

Figure 12b. Influence of excitational acceleration on induced buoyancy force on bubble in sinusoidally excited vertical tank
(Bubble at medium depth)

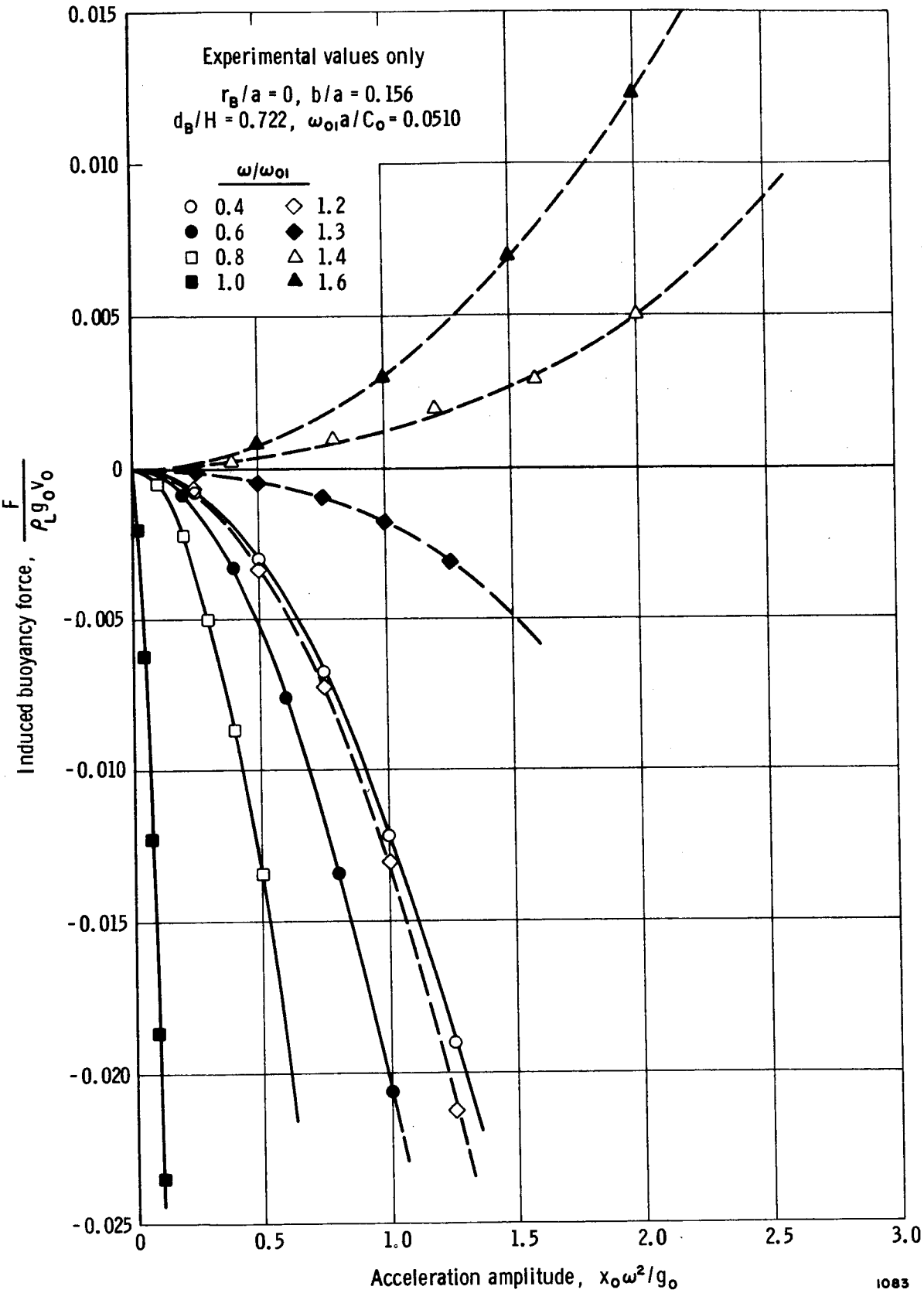

Figure 12c. Influence of excitational acceleration on induced buoyancy force on bubble in sinusoidally excited vertical tank
(Bubble near tank bottom)

each curve is for a fixed input frequency, while input acceleration is varied. It is interesting to note that each curve appears to be a parabola of some form. Further, negative forces are experienced for excitational frequencies below $\omega/\omega_{o1} = 1.0$, while positive forces can be experienced for frequencies above this, depending on the depth of the bubble. These results clearly indicate the influence of the direction of the pressure gradient on the direction of resulting average force. Damping in the system results in the $\omega/\omega_{o1} = 1.0$ curve not exactly coinciding with the negative ordinate axis. It should be emphasized that, in each part of Figure 12a, b, or c, the ratio ω/ω_{o1} is based on the first mode natural frequency corresponding to the bubble depth for that figure. Thus, ω_{o1} varies from one depth to the other, as indicated in the middle curve in Figure 8.

It now becomes pertinent to determine the range of bubble sizes over which the small bubble theory will give a reasonable approximation to average induced vibrational force. For this purpose, a comparison of results predicted by Equation (16) with experimental data is shown in Figure 13. Here also, as in Figure 8, it can be seen that a bubble size of about $b/a = 0.05$ is the limit, beyond which the small bubble theory no longer gives a good approximation to the bubble behavior. The downward curvature of the theoretical curves is a result of the coupled bubble resonance, mentioned previously. Again, it can be seen that no such behavior occurred experimentally. It may be noted that, if the assumption $\omega << \Omega_B$ is made in Equation (16), then the force is independent of bubble size, and the results from the small bubble theory become a series of horizontal straight lines, each passing through its respective value at $b/a = 0$ in Figure 13. Thus, an even better correlation with the experimental results would be achieved up to a bubble size of about $b/a = 0.2$ for the cases shown. This result is consistent with the previous comments regarding surface tension effects.

Several cautions should be exercised in interpreting the results indicated in Figure 13. The form of captive bubble used for the experiments undoubtedly influences the results to some presently unknown extent. One indication of this influence is the fact that a value of $\gamma = 1.4$ rather than $\gamma = 1.0$ had to be used to compute the theoretical curves in order for the results to fall near each other. This, of course, is contrary to what has been determined in previous studies, as was mentioned in the introduction. However, as has been mentioned, the balloon added stiffness to the bubble, and increasing the factor γ would tend to allow for this increase. Further, data of this type should be compared over a wider range of frequencies before a complete confidence can be given to the conclusions that the figure points toward. However, it is felt at the moment that a bubble size of $b/a \leq 0.05$ probably is a reasonable limit for the application of the small bubble theory.

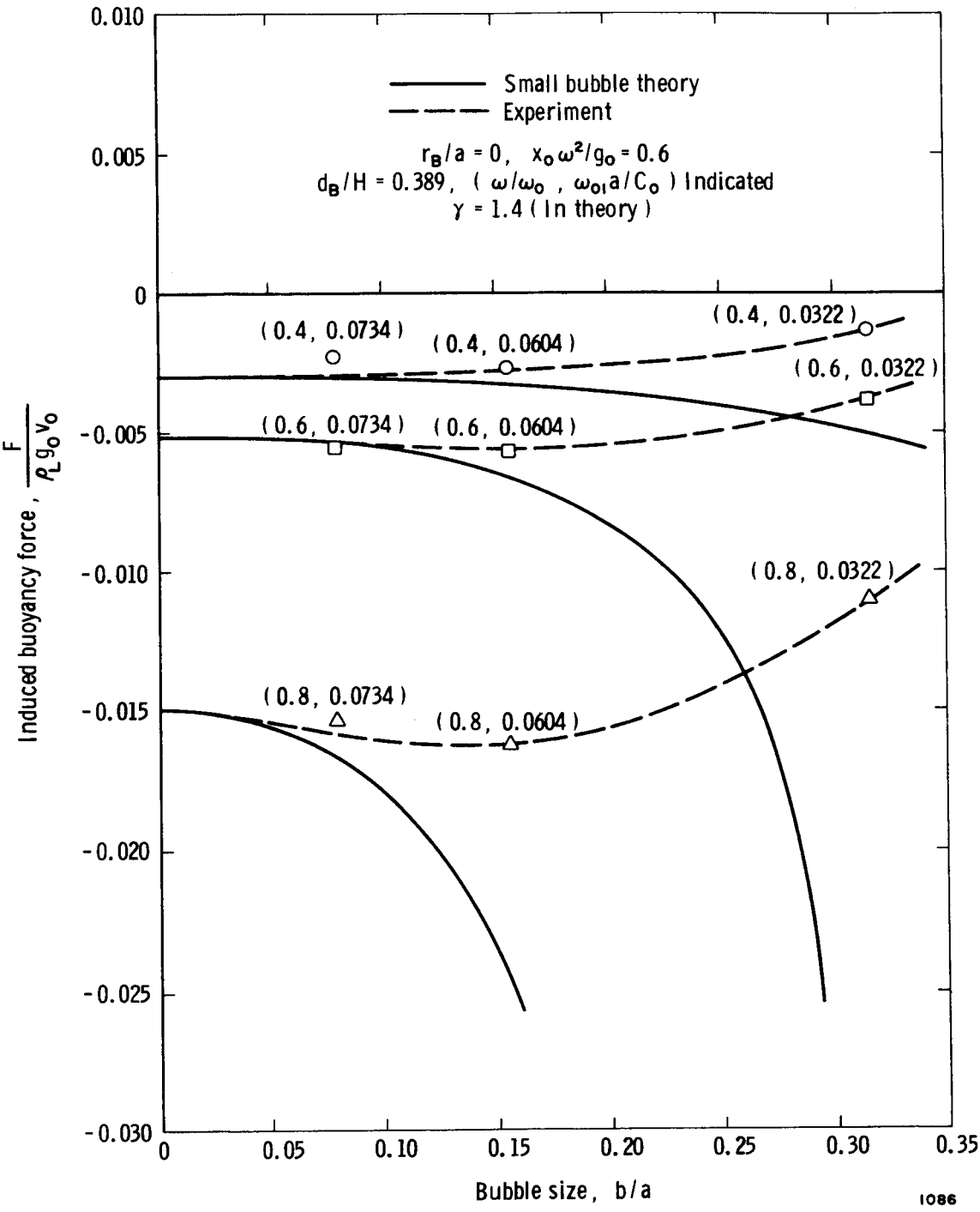

Figure 13. Influence of bubble size on induced buoyancy force on bubble in sinusoidally excited vertical tank

In order to get some idea of the amplitudes of input acceleration that can influence bubbles in a low gravity environment, numerical results based on Equation (18) are shown in Figure 14. The various fixed parameters were chosen as typical for a prototype system in earth orbit, and excitational frequencies are below and in the vicinity of the first natural mode of the system ($\phi = \pi$). For a given curve at a given depth, all bubbles will rise for input accelerations below the curve, and will sink for accelerations above the curve. Thus, bubbles may collect at various depths, depending on the frequency of excitation. It can be seen that very low input accelerations are required to move the bubbles about. Although a factor of $\gamma = 1.4$ has been used in computing these results, they are nearly the same for $\gamma = 1.0$ in this case, as can be seen from Equation (18). In Reference [7], a similar plot has been given for bubble behavior in a 1-g_o environment.

Bubble Force for Random Excitation. Average induced buoyancy force measured under random excitation is shown in Figure 15 for other conditions that were similar to those in Figure 12. In this case, however, the acceleration is rms - g_o's, and the frequency parameter ω/ω_{o1} is based on the center of the 20-cps random bandwidth excitation. Further, the measured force in this case continued to fluctuate randomly, and an average of this fluctuation was measured, whereas the average force assumed a steady value for pure sinusoidal excitation. In general, it can be seen that, qualitatively, similar results are displayed in the bubble behavior, even under random excitation. An important consideration, of course, is that random excitation does not necessarily produce random response, as is the case here where a definite average force appeared. It may also be suspected that the pressure response in the system itself acts as a mechanical filter, favoring those frequencies near the natural modes of the system. The responses at these frequencies then have the more pronounced effect on the bubble behavior.

Horizontal Orientation

As was mentioned previously, force data were not obtained for the bubble in the horizontally oriented tank because of the inaccessibility of the bubble for this case. The tests were conducted primarily to obtain qualitative indications of the behavior of a more representative system for the case where a ullage bubble exists in the tank under low gravity. Of course, the horizontal component of gravity was truly zero in this case. The feasibility of the use of this arrangement for further studies of bubble behavior at simulated low gravity conditions was readily demonstrated. Quantitative natural frequency data were obtained for the system experimentally and will now be presented.

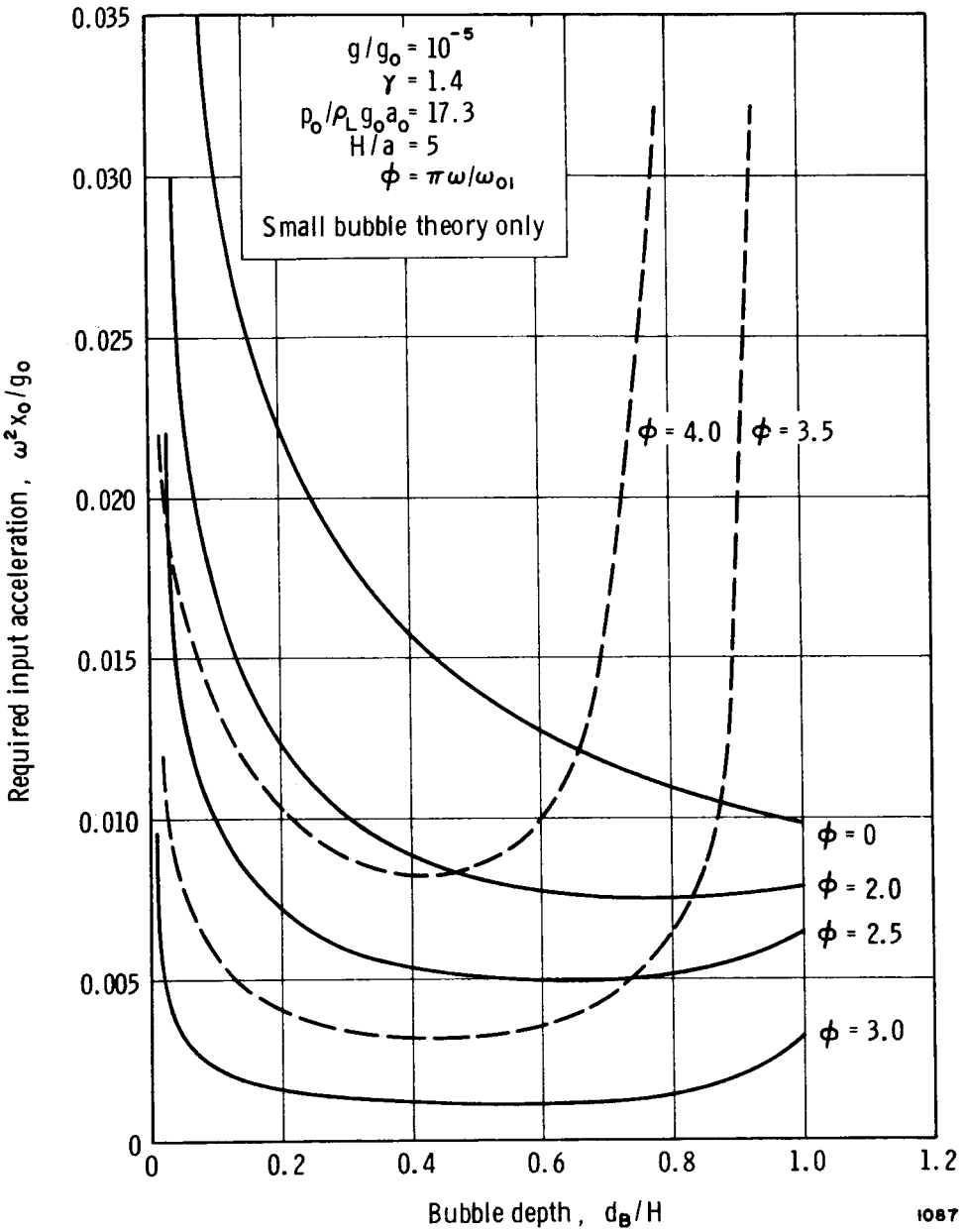

Figure 14. Input acceleration required to overcome steady buoyancy force on bubble in a low gravity environment

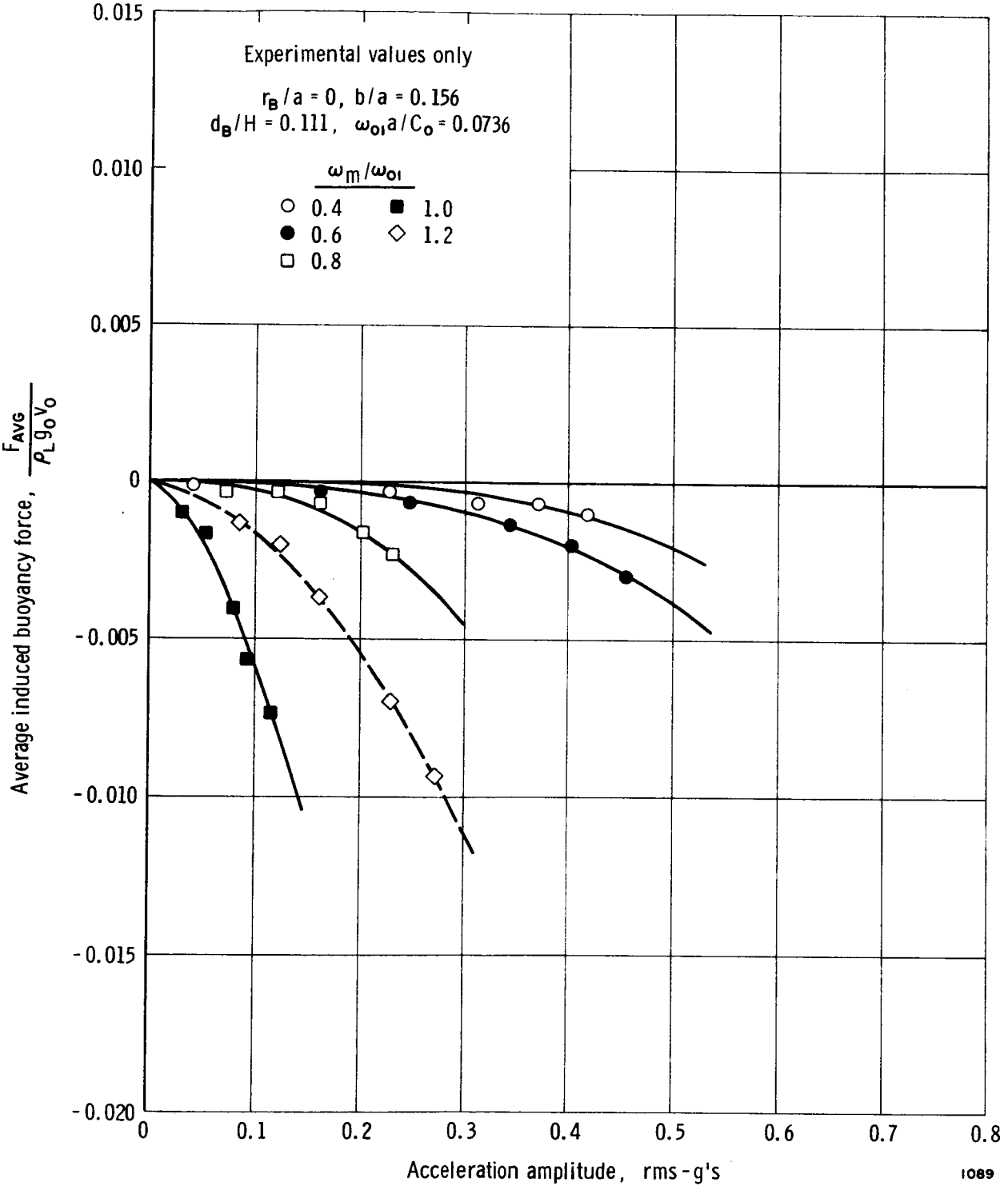

Figure 15a. Influence of excitational acceleration on average induced buoyancy force on bubble in randomly excited vertical tank
(Bubble near liquid surface)

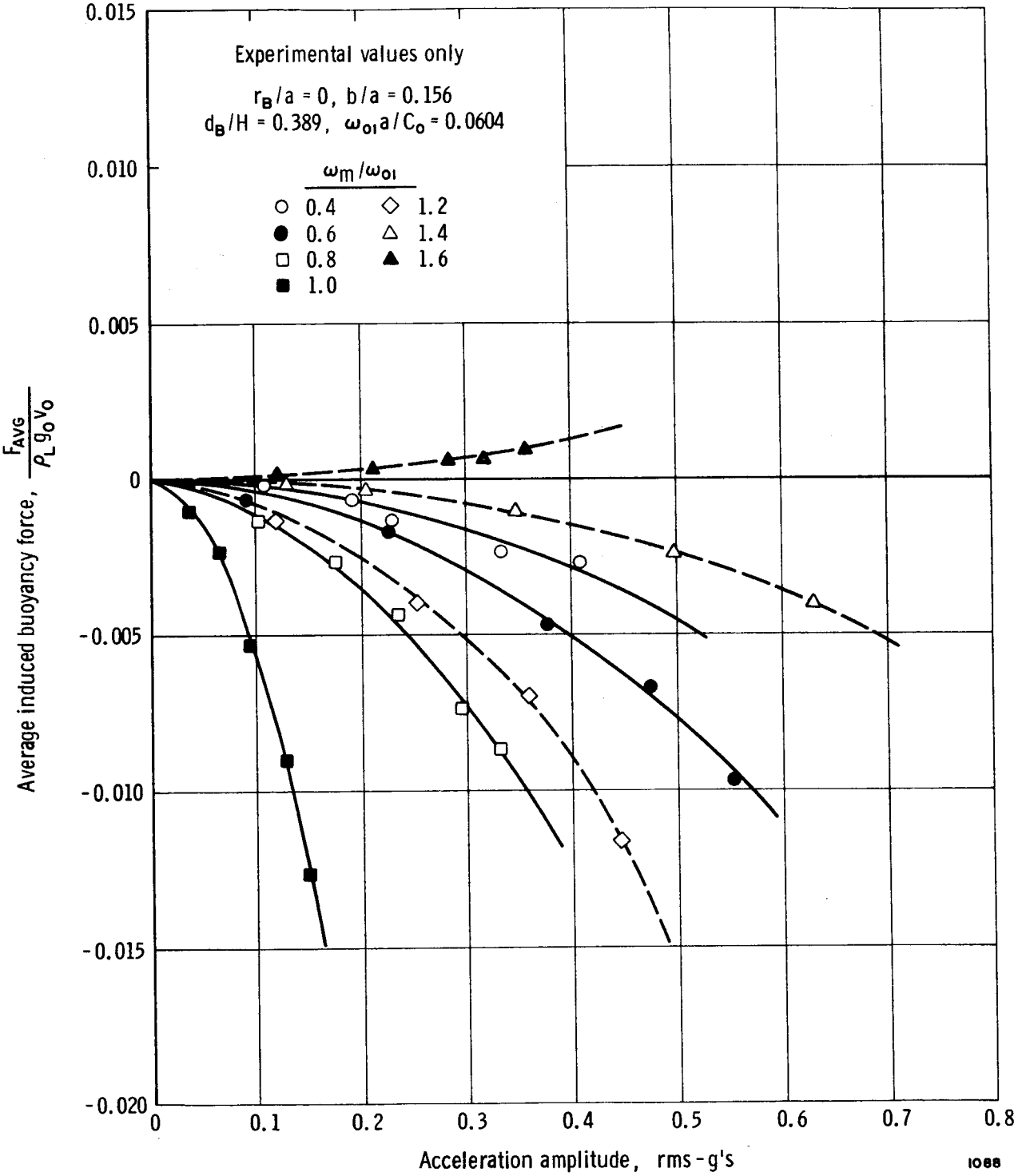

Figure 15b. Influence of excitational acceleration on average induced buoyancy force on bubble in randomly excited vertical tank
(Bubble at medium depth)

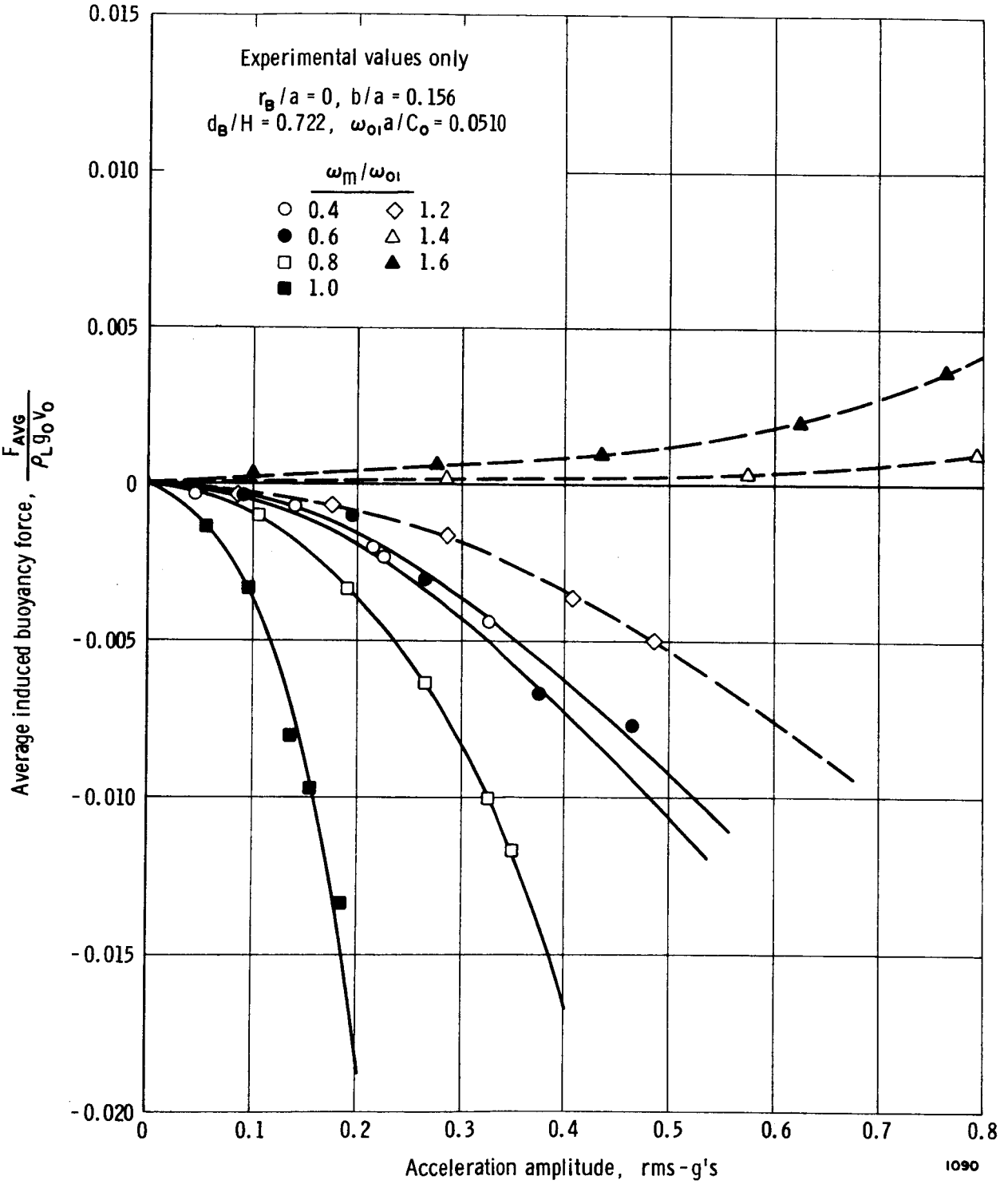

Figure 15c. Influence of excitational acceleration on average induced buoyancy force on bubble in randomly excited vertical tank
(Bubble near tank bottom)

The pressure distribution along the tank axis is shown in Figure 16 for the first two axisymmetric modes in this system where no bubble is present in the tank. The free ends of the tank are reflected in the shape of the pressure wave. Ideally, it would appear that these modes should be symmetrical about the tank center. The distortion may have resulted through the influence of the tank support and excitation system. These pressure distributions, of course, correspond to those shown in Figure 7 for the vertically oriented, closed-open tank having a free surface.

The effect of bubble size and axial position on natural frequency is shown in Figure 17 for the first mode only. Here also, it can be seen that the presence of the bubble compliance has the least influence on the system when the bubble is near the antinode of the undistorted pressure distribution. Some idea of the distortion in the pressure wave can be obtained from Figure 18, where the pressure nodal position is plotted against bubble axial position. All measurements were made with the bubble on the centerline of the tank.

With the system in the horizontal orientation, all sizes of captive bubbles could readily be moved about to various axial locations in the tank, depending on the excitational conditions. Acceleration inputs of as little as $0.05\text{-}g_o$ could cause the bubbles to move for frequencies near a natural mode, providing that the bubble was not initially located at an equilibrium position. In general, the bubbles would move toward the points of increasing pressure amplitude (against the pressure gradient), a result which fully agrees with earlier observations in other systems. However, in this case where the bubble was allowed to move, the natural frequency of the system would change accordingly. Thus, under certain conditions, the bubble motion would accelerate, from unstable positions for a constant input amplitude. It could readily be seen that bubbles would tend to collect at definite locations in the tank, depending on the input conditions. Similar behavior was also observed qualitatively in this tank for random input conditions.

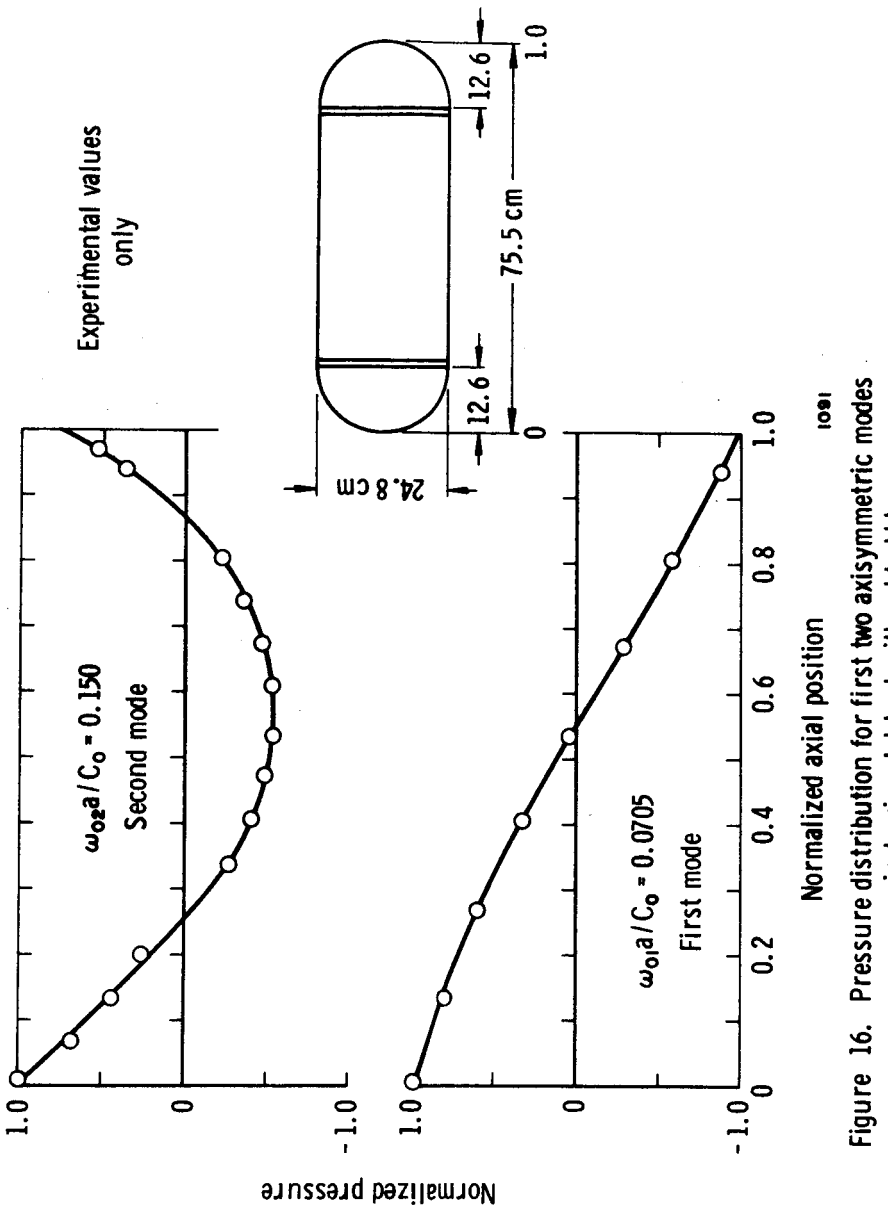

Figure 16. Pressure distribution for first two axisymmetric modes in horizontal tank without bubble

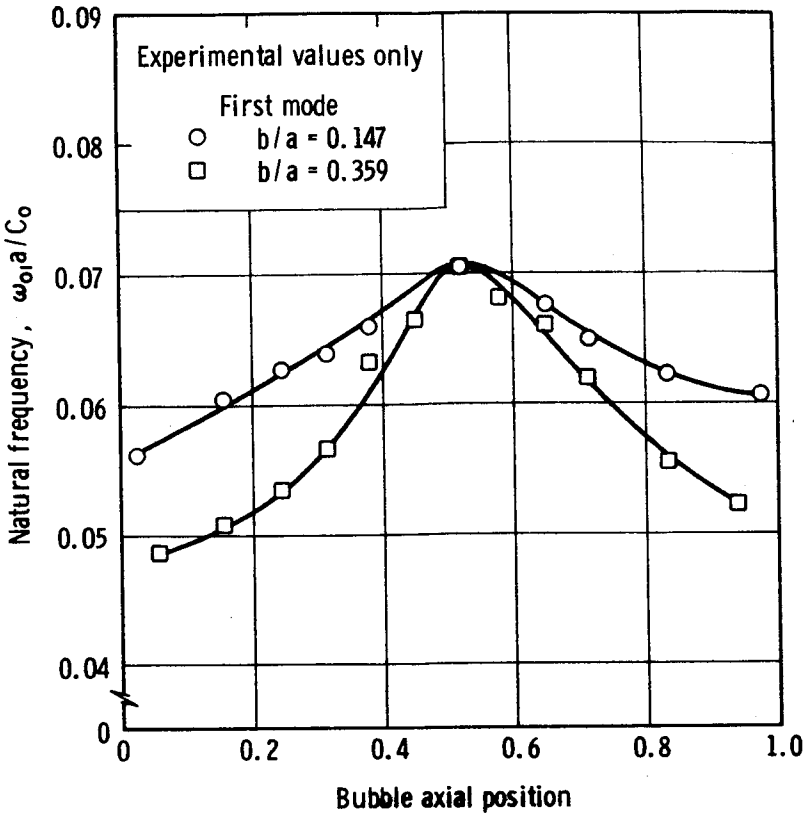

Figure 17. Variation of first mode natural frequency with bubble location in horizontal tank

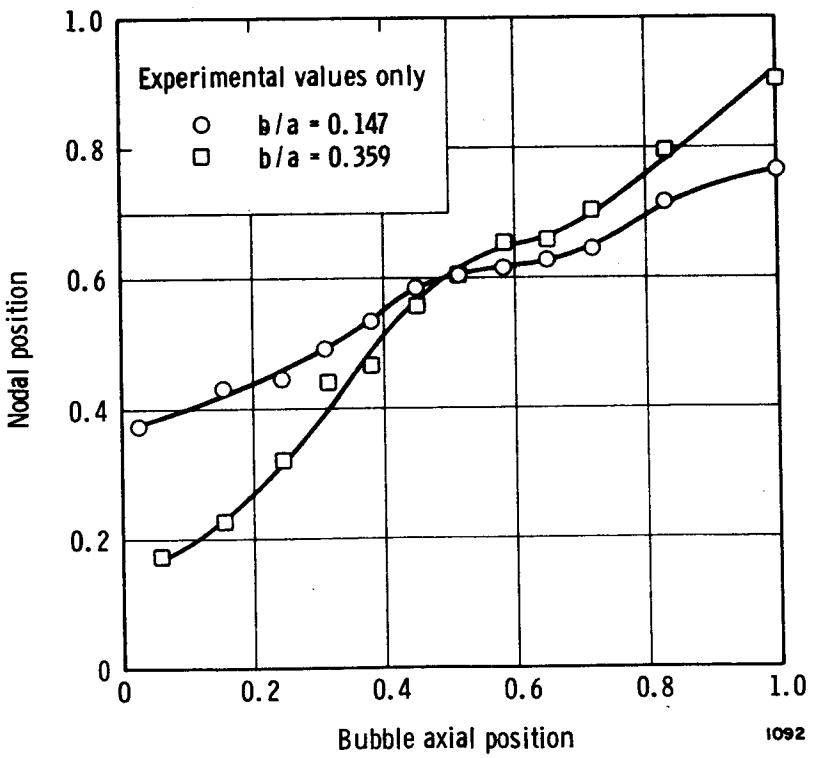

Figure 18. Variation of pressure nodal position with bubble location in horizontal tank

V. DISCUSSION

The finite-bubble theory developed in the present work, in essence, is an extension of previous results that have been developed for small bubbles only. One complements the other in that each appears to give useful results over different ranges of bubble size. Similar restrictions apply to both theories, however, in that they are directly applicable only to axisymmetric pressure distributions that can be expressed in terms of plane water-hammer waves, and both are influenced by the theoretical bubble mode, the true value of which remains uncertain. It is believed that, by including surface tension effects, the results for small bubbles could be improved considerably.

Recent work on axisymmetric modes of oscillation in tanks of representative space vehicle geometry indicates that the plane wave pressure distribution assumption is not particularly good at liquid depths in the range $H/a < 2$. In view of the methods required to solve even the simplified case for a finite bubble size, it is obvious that extreme difficulty will be encountered in developing a more accurate theory, and finite element numerical techniques employing small mesh sizes will have to be used in the solution of the equations. However, it appears that a complete prediction of bubble behavior under given conditions of vibration can be obtained in no simpler fashion.

It should be emphasized that, to date, very little work has been accomplished in studying bubble behavior in tanks that are vibrating in non-axisymmetric modes. No work at all has been done for the case of bubbles in a tank vibrating in nonlinear modes. Of course, a vehicle liquid-tank system can respond in several types of modes, each of which probably will cause different patterns of bubble migration. Even for the case of small bubbles, the main problem appears to be in first predicting the pressure distribution within the liquid, for whatever kind of mode the system may be experiencing. This can be a formidable task itself, and the addition of finite bubble size, then, further complicates the problem.

Upon comparing the present results of the small bubble and finite bubble theories for axisymmetric responses, it appears that useful approximations can be obtained from the simpler theory for bubble sizes up to about $b/a = 0.05$. This result is quite significant when it is realized that the limit already represents a bubble of about 0.5-meter diameter in a tank of the size of those used in an S-IC booster. In fact, a single bubble of that size probably would not exist in a vibrational environment but would break up into a cluster of smaller bubbles. However, according to Bleich's approximations, the behavior of the cluster would be similar to that of a single large bubble

of the same size. Obviously, bubbles or clusters of this size already are large enough to be a hazard in the propulsion system of the vehicle.

The fact that bubbles can be moved about with random inputs, and that low inputs are required under low gravity conditions is most significant. This definitely points toward potential problems being caused by migrating bubbles under orbital conditions. Again, however, the pressure response in the tank must be considered in order to gain even a qualitative idea of the bubble migration pattern. Unfortunately, the pressure response depends greatly on the kind of excitation as well as how it is applied to the tank. In other words, the effects of on-board noise sources in orbit must be evaluated.

Orienting an experimental tank horizontally appears to be a very good way of simulating low gravity conditions under which to study longitudinal migration of bubbles. Of course, the approximations involved in the use of captive bubbles are inherent; however, much can be learned from more work with such an apparatus. Bubble motion under either sinusoidal or random inputs can readily be evaluated for excitational inputs at virtually any location on the tank if suitable supporting fixtures are provided.

In general, it may be concluded that the present work has served to point out the definite potential of bubble behavior as a problem under low gravity conditions, and that a good knowledge of this behavior under various environmental conditions can be gained only at the expense of considerably more work, both theoretical and experimental.

ACKNOWLEDGMENTS

The authors wish to express their sincere appreciation to Drs. H. N. Abramson, F. T. Dodge, and C. R. Gerlach for consultation regarding the conduct of this research effort, and to Mr. D. C. Scheidt for conducting most of the experiments. The efforts of Mr. Richard Gunst and the SwRI computations laboratory are also gratefully acknowledged.

REFERENCES

1. Dodge, F. T., "A Review of Research Studies on Bubble Motion in Liquids Contained in Vertically Vibrating Tanks," Technical Report No. 1, Contract No. NAS8-11045, Southwest Research Institute, San Antonio, Texas, December 1963.

2. Fritz, C. G., "A Study of Bubble Motion in Liquid Nitrogen," Advances in Cryogenic Engineering, Volume II, Editor - Timmarhaus, Plenum Press, New York, pp. 584-592 (1966).

3. Kana, D. D., "Longitudinal Dynamics of Liquid Filled Elastic Shells," Summary Report, Contract No. NAS8-11045, Southwest Research Institute, San Antonio, Texas, September 1966.

4. Dachs, Louis L., "Handling Liquid Prepellants," Space/Aeronautics, 46, 5, pp. 77-84, October 1966.

5. Bleich, H. H., "Effect of Vibrations on the Motion of Small Gas Bubbles in a Liquid," Jet Propulsion, 26, pp. 958-978, November 1956.

6. Bleich, H. H., "Motions of Clusters of Gas Bubbles in Vibrated Vessels," Report No. GM-TR-27, Contract No. AF(600)-1190, Ramo-Wooldridge Corporation, April 1956.

7. Kana, D. D., and Dodge, F. T., "Bubble Behavior in Liquids Contained in Vertically Vibrated Tanks," Technical Report No. 4, Contract No. NAS8-11045, Southwest Research Institute, San Antonio, Texas, August 1964; also Journal of Spacecraft and Rockets, 3, 5, pp. 760-763, May 1966.

8. Plesset, M. S., and Hsieh, D. Y., "Theory of Gas Bubble Dynamics in Oscillating Pressure Fields," The Physics of Fluids, 3, 6, pp. 882-892, November-December 1960.

9. Fritz, C. G., Ponder, C. A., Jr., and Blount, D. H., "Bubble Coalescense in a Longitudinally Vibrated Column," Proceedings of the ASME Symposium on Cavitation in Fluid Machinery, ASME, New York (1965).

10. Schoenhals, R. J., and Overcamp, T. J., "Pressure Distribution and Bubble Formation Induced by Longitudinal Vibration of a Flexible Liquid-Filled Cylinder," NASA TM X-53353, George C. Marshall Space Flight Center, Huntsville, Alabama, September 1965.

11. Kana, D. D., and Abramson, H. N., "Longitudinal Vibration of Ring Stiffened Cylindrical Shells Containing Liquids," Technical Report No. 7, Contract No. NAS8-11045, Southwest Research Institute, San Antonio, Texas, June 1966.

12. Reissner, E., "Notes on Forced and Free Vibrations of Pressurized Cylindrical Shells Which Contain a Heavy Liquid with a Free Surface," Report No. GM-TR-87, AMNO 6-15, Contract No. AF 18-(600)-1190, Guided Missile Division, TRW Space Technology Laboratories, November 1956.

13. Tarrantine, F. J., "Unconventional Methods for Influencing Fluid Flow," AFAPL-TR-64-133, Part V, Carnegie Institute of Technology, November 1965.

14. Lamb, Sir Horace, Hydrodynamics, Sixth Edition, Dover Publications, New York, p. 7 (1932).

APPENDIX

1. Quasi-One-Dimensional Flow Equation
2. Evaluation of Induced Buoyancy Force
3. Numerical Solution for Natural Frequencies
4. Numerical Solution for Induced Buoyancy Force

APPENDIX

1. Quasi-One-Dimensional Flow Equation

An equation for average flow will be determined for the region occupied by the liquid. Consider cylindrical coordinates with origin located in some cross section which cuts through the bubble in the tank as shown in Figure A-1. Let the shaded area which includes the liquid only be

$$A = A_2 - A_1$$

In this region, the continuity equation applies

$$\frac{\partial \rho}{\partial t} + \rho_L \operatorname{div} \vec{u} = 0$$

In order to consider the average flow through the shaded area, we may integrate this equation to obtain

$$\frac{\partial \rho}{\partial t} + \frac{\rho_L}{A} \int_{A_2} \operatorname{div} \vec{u}\, dA_2 - \frac{\rho_L}{A} \int_{A_1} \operatorname{div} \vec{u}\, dA_1 = 0 \qquad (A1)$$

Considering the cylindrical coordinates located at the center of A_i (either A_1 or A_2), we may write

$$\int_{A_i} \operatorname{div} \vec{u}\, dA_i = \left[\int_0^{2\pi} (r u_r) d\theta + \int_0^{2\pi} \left[- u_\theta \frac{\partial R_i}{\partial \theta} \right] d\theta - \int_0^{2\pi} \left(u_x R_i \frac{\partial R_i}{\partial x} \right) d\theta + \frac{\rho_L}{A} \frac{\partial q_i}{\partial x} \right]_{r = R_i} \qquad (A2)$$

where

$$q_i = \int_{A_i} u_x dA_i$$

and

$$q = q_2 - q_1$$

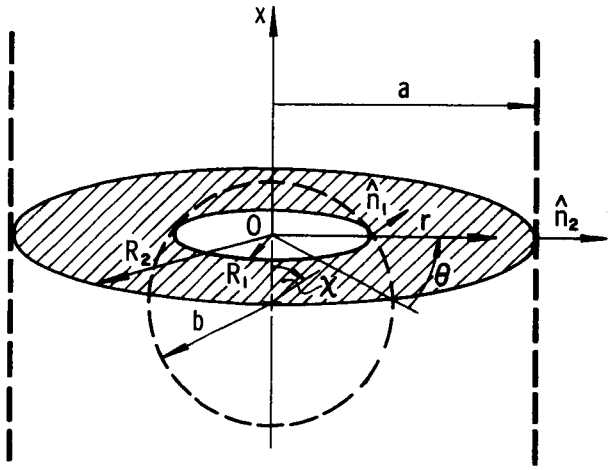

Figure A-1

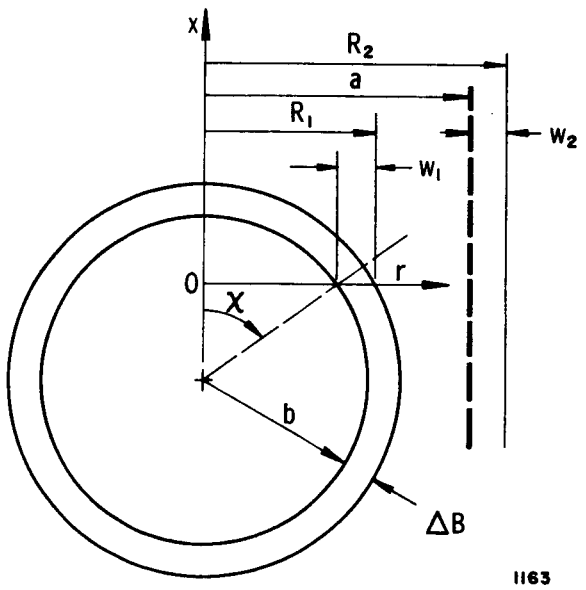

Figure A-2

In order to evaluate the above integrals, we consider the boundaries of the liquid. The shaded area of liquid is dependent on two geometrical boundaries (1 and 2). In the specified cylindrical coordinate system, we can write them as

$$F_i = r - R_i(\theta, x, t) = 0$$

Since

$$dF_i = \frac{\partial F}{\partial r} dr + \frac{1}{r} \frac{\partial F}{\partial \theta} r d\theta + \frac{\partial F}{\partial x} dx$$

the function F_i increases along the normals which have direction cosines

$$[\cos(\hat{n}_i, r), \cos(\hat{n}_i, \theta), \cos(\hat{n}_i, x)] = \frac{1}{G}\left[1, -\frac{1}{r}\frac{\partial R_i}{\partial \theta}, -\frac{\partial R_i}{\partial x}\right]$$

where

$$G = \sqrt{1 + \left(\frac{1}{r}\frac{\partial R_i}{\partial \theta}\right)^2 + \left(\frac{\partial R_i}{\partial x}\right)^2}$$

From Figure A2, it can be seen that

$$\frac{\partial R_i}{\partial t} = \frac{\partial w_i}{\partial t} .$$

Thus, as in Lamb [14], we may equate the normal velocity of the boundary (i) to the normal velocity of the fluid at the boundary (i)

$$\dot{u}_{ni} = -\frac{1}{G}\frac{\partial F_i}{\partial t} = \frac{1}{G}\frac{\partial w_i}{\partial t} = u_r \cos(\hat{n}_i, r) + u_\theta \cos(\hat{n}_i, \theta) + u_x \cos(\hat{n}_i, x)$$

or

$$\left[r u_r - u_\theta \frac{\partial R_i}{\partial \theta} - u_x \frac{\partial R_i}{\partial x} = r \frac{\partial w_i}{\partial t}\right]_{r = R_i}$$

Thus, we may write Equation (A2) as

$$\int_{A_i} \operatorname{div} \vec{u}\, dA_i = \int_0^{2\pi} R_i \frac{\partial w_i}{\partial t} d\theta = 2\pi R_i \frac{\partial w_i}{\partial t}$$

so that Equation (A1) becomes

$$\frac{\partial \rho}{\partial t} + \frac{\rho_L}{A}\frac{\partial q}{\partial x} + 2\pi \frac{\rho_L}{A}\left(R_2 \frac{\partial w_2}{\partial t} - R_1 \frac{\partial w_1}{\partial t}\right) = 0$$

From Figure A-2, it can be seen that

$$\frac{\partial w_1}{\partial t} = \frac{\partial \Delta_B}{\partial t} \sin \chi \quad , \quad R_1 \cong b \sin \chi$$

and

$$\frac{\partial w_2}{\partial t} = \frac{\partial w}{\partial t} \quad , \quad R_2 = a$$

Hence, we obtain

$$\frac{\partial \rho}{\partial t} + \frac{\rho_L}{A}\frac{\partial q}{\partial x} + 2\pi \frac{\rho_L}{A}\left(A \frac{\partial w}{\partial t} - b \sin^2 \chi \frac{\partial \Delta_B}{\partial t}\right) = 0 \qquad (6)$$

2. Evaluation of Induced Buoyancy Force

The time average of the vertical force on a bubble in a vibrated liquid (Fig. 1b) is

$$F = -\overline{2\pi \int_0^{\pi} p(\xi_1)(b + \Delta_B)^2 \sin \chi \cos \chi \, d\chi}$$

By noting that

$$\xi_1 = \xi + \Delta_B \cos \chi$$

and using the first two terms of the Taylor expansion,

$$p(\xi_1) = p(\xi) + \frac{\partial p}{\partial \xi}(\xi_1 - \xi) + \cdots$$

and, noting that $p(\xi)$ and Δ_B are periodic in time, we may write

$$F = -2\pi b \hat{\Delta}_2 \int_0^{\pi} \hat{p}(\xi) \cos \chi \sin \chi \, d\chi - \pi b^2 \hat{\Delta}_B \int_0^{\pi} \frac{\partial \hat{p}}{\partial \xi} \cos^2 \chi \sin \chi \, d\chi$$

Now, note that

$$\xi = b \cos \chi$$

and, from integration by parts, we have

$$\int_0^{\pi} \hat{p}(\xi) \cos \chi \sin \chi \, d\chi = -\frac{1}{2}\left[\hat{p} \cos^2 \chi\right]_0^{\pi} - \frac{b}{2}\int_0^{\pi} \frac{d\hat{p}}{\partial \xi} \cos^2 \chi \sin \chi \, d\chi$$

and the average force may therefore be expressed as

$$F = -\pi b \hat{\Delta}_B \left[\hat{p}(b) - \hat{p}(-b)\right]$$

and, nondimensionalizing, it becomes

$$\frac{F}{\rho_L g_o v_o} = -\frac{3}{4}\frac{a^2}{b^2}\left[\hat{p}^*\left(\frac{b}{a}\right) - \hat{p}^*\left(-\frac{b}{a}\right)\right]\hat{\Delta}_B^* \qquad (13a)$$

3. Numerical Solution for Natural Frequencies

A seminumerical procedure is employed in solving Equation (11). For the assumed condition of plane-wave flow, the simple sine and cosine solutions for the liquid column that are subject to the conditions

$$p^* = 0 \text{ at } x^* = \frac{H}{a}$$

$$\frac{\partial p^*}{\partial x^*} = -\frac{x_o \omega^2}{g_o} \cos \omega t \text{ at } x^* = 0$$

are, for below the bubble,

$$p^* = K_2^* \sin(\Omega_e x^*) \quad \text{for } x^* < x^-/a$$

where

$$K_2^* = -\frac{x_o \omega^2}{\Omega_e g_o}, \quad \Omega_e = \frac{\omega a}{C_e}, \quad x^- = H - d_B - b$$

and, for above the bubble,

$$p^* = K_3^* \sin\left[\Omega_e \frac{(x - H)}{a}\right] \quad \text{for } x^* > x^+/a$$

where

$$K_3^* = p^* \left(\frac{x^+}{a}\right) \Big/ \sin\left[\Omega_e \frac{x^+ - H}{a}\right], \quad x^+ = H - d_B + b$$

These equations become boundary conditions for the bottom and top of the bubble, respectively, and a numerical solution is now carried out for the region including the bubble.

Using central difference formulas and taking net points at the centers of each interval across the bubble region, Equation (11a) reduces to the difference equation

$$\frac{p_{n+1} - 2p_n + p_{n-1}}{\Delta^2} + \frac{\partial A^*}{A^* \partial x^*}\left[\frac{p_{n+1} - p_{n-1}}{2\Delta}\right] + \frac{1}{C_{eB}^{*2}} \lambda^2 p_n = 0$$

where

$$\lambda_i^2 = \frac{\omega_{oi}^2 a^2}{C_o^2}$$

and it is now understood that the pressures are nondimensional (p*'s). By using N increments in the bubble region, the resulting N equations can be expressed in matrix form as

$$\left\{[A] - \lambda^2 [B]\right\} [P] = [C]$$

where

$$[P] = \begin{Bmatrix} p_1 \\ p_2 \\ \cdot \\ \cdot \\ \cdot \\ p_N \end{Bmatrix}$$

and [C] is a column matrix made up of the constants resulting from applying the boundary conditions at $\xi^* = \pm b/a$. [A] and [B] are square matrices. For convenience in expressing the elements of these matrices, we define the following quantities:

$$A'_{n,\ n+1} = 1 + \frac{\Delta}{2} F_n \quad ; \quad F_n = \frac{1}{A^*} \frac{\partial A^*}{\partial x^*}$$

$$A'_{n,\ n-1} = 1 - \frac{\Delta}{2} F_n$$

$$A'_{n,\ n} = -2$$

$$B'_{n,\ n} = -\frac{\Delta^2}{C^{*2}_{eB}}$$

where

$$\Delta = \frac{2b}{aN} \quad , \quad \Omega_e = \frac{\omega a}{C_e}$$

We now consider the elements of [A] and [B] for separate cases of n.

1) For $2 \leq n \leq N - 1$:

$$A_{n,\ n+1} = A'_{n,\ n+1}$$

$$A_{n,\ n-1} = A'_{n,\ n-1}$$

$$A_{n,\ n} = A'_{n,\ n}$$

$$B_{n,\ n} = B'_{n,\ n}$$

Other elements are zero.

2) For n = 1:

$$A_{n,\ n+1} = A'_{n,\ n+1}$$

$$A_{n,\ n} = A'_{n,\ n} + \left(A'_{n,\ n-1}\right) \left[\frac{1 + \frac{\Delta}{2} \Omega_e \tan\left(\Omega_e \frac{x^-}{a}\right)}{1 - \frac{\Delta}{2} \Omega_e \tan\left(\Omega_e \frac{x^-}{a}\right)} \right]$$

This is because

$$p_o^* = p_1^* \left[\frac{1 + \frac{\Delta}{2} \Omega_e \tan\left(\Omega_e \frac{x^-}{a}\right)}{1 - \frac{\Delta}{2} \Omega_e \tan\left(\Omega_e \frac{x^-}{a}\right)} \right]$$

derived from

$$(p^*)_{x^* = x^-/a} \cong \frac{1}{2} (p_o^* + p_1^*)$$

$$\frac{p_1 - p_o}{\Delta} \cong \left(\frac{\partial p^*}{\partial x^*}\right)_{x^* = x^-/a} = \frac{- \Omega_e (p^*)_{x^* = x^-/a} \sin\left(\Omega_e \frac{x^-}{a}\right)}{\cos\left(\Omega_e \frac{x^-}{a}\right)} - \frac{x_o \omega^2}{g_o} \frac{1}{\cos\left(\Omega_e \frac{x^-}{a}\right)}$$

$$B_{n,\,n} = B'_{n,\,n}$$

$$C_n = \left(A'_{n,\,n-1}\right) \left[\frac{+ \Delta \frac{x_o \omega^2}{g_o}}{\cos\left(\Omega_e \frac{x^-}{a}\right)} \right] \Bigg/ \left[1 - \frac{\Delta}{2} \Omega_e \tan\left(\Omega_e \frac{x^-}{a}\right) \right]$$

Other elements are zero.

3) For n = N,

$$A_{n,\,n-1} = A'_{n,\,n-1}$$

$$A_{n,\,n} = A'_{n,\,n} + \left(A'_{n,\,n+1}\right) \frac{1 + \frac{\Delta \Omega_e}{2} \cot\left(\Omega_e \frac{x^+ - H}{a}\right)}{1 - \frac{\Delta \Omega_e}{2} \cot\left(\Omega_e \frac{x^+ - H}{a}\right)}$$

This is because

$$\left(P_N + 1\right) \left[1 - \frac{\Delta \Omega_e}{2} \cot\left(\Omega_e \frac{x^+ - H}{a}\right) \right] = P_N \left[1 + \frac{\Delta \Omega_e}{2} \cot\left(\Omega_e \frac{x^+ - H}{a}\right) \right]$$

derived from:

$$\frac{P_{N+1} - P_N}{\Delta} \cong \left(\frac{\partial p^*}{\partial x^*}\right)_{x^* = x^+/a} = \frac{P_N + P_{N+1}}{2} \frac{\Omega_e \cos\left(\Omega_e \frac{x^+ - H}{a}\right)}{\sin\left(\Omega_e \frac{x^+ - H}{a}\right)}$$

as pressure is zero at the liquid surface, x = H. And

$$B_{n,n} = B'_{n,n}$$

$$C_n = 0$$

All other elements are zero.

4. Numerical Solution for Induced Buoyancy Force

Equations (13) must be solved numerically using the same matrices given above. However, we now specify a given excitational frequency (ω), hence a given λ, and must solve Equations (11) for the appropriate pressures in the region occupied by the bubble. Thus, we must numerically solve

$$[P] = \left\{[A] - \lambda^2[B]\right\}^{-1}[C]$$

and the results are used to solve Equations (13a), (13b), and (13c) numerically.